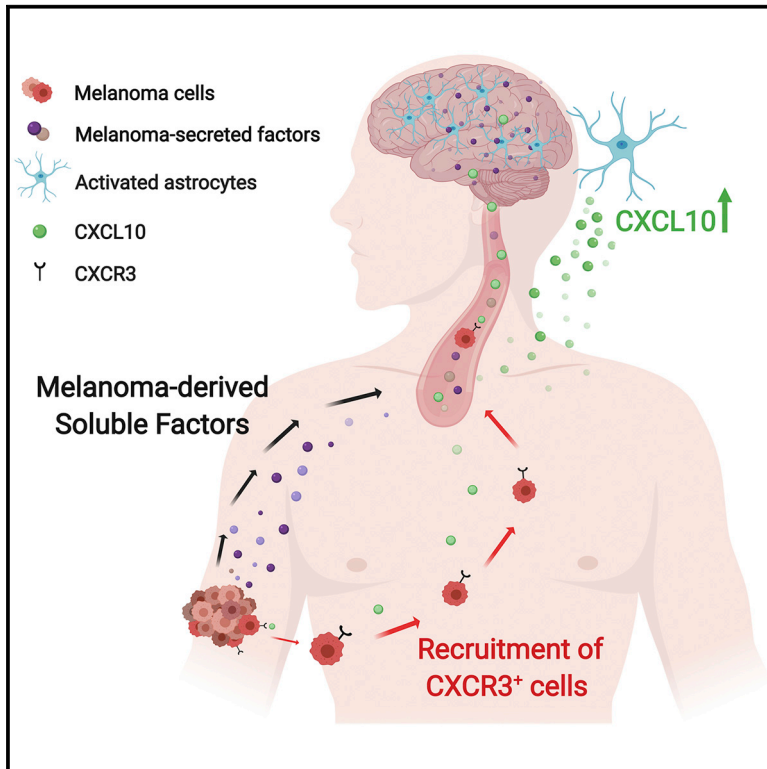


## Inflammatory Activation of Astrocytes Facilitates Melanoma Brain Tropism via the CXCL10-CXCR3 Signaling Axis

### Graphical Abstract



### Authors

Hila Doron, Malak Amer, Nour Ershaid, ..., Ronit Satchi-Fainaro, Tobias Pukrop, Neta Erez

### Correspondence

netaerez@tauex.tau.ac.il

### In Brief

Melanoma brain metastases are incurable. Doron et al. find that astrocyte-secreted CXCL10 is functional in melanoma chemoattraction to the brain. CXCR3, the CXCL10 receptor, is upregulated in brain-seeking melanoma cells. Silencing CXCR3 expression attenuates brain metastasis, suggesting that the CXCL10-CXCR3 axis may be a therapeutic target for melanoma brain metastasis.

### Highlights

- CXCL10 is upregulated in metastases-associated astrocytes *in vivo*
- Astrocyte-derived CXCL10 enhances melanoma cell migration toward astrocytes
- CXCR3, the receptor for CXCL10, is upregulated in brain-tropic melanoma cells
- Targeting CXCR3 expression attenuates the formation of melanoma brain metastases



# Inflammatory Activation of Astrocytes Facilitates Melanoma Brain Tropism via the CXCL10-CXCR3 Signaling Axis

Hila Doron,<sup>1,8</sup> Malak Amer,<sup>1,8</sup> Nour Ershaid,<sup>1</sup> Raquel Blazquez,<sup>2</sup> Ophir Shani,<sup>1</sup> Tzliil Gener Lahav,<sup>1</sup> Noam Cohen,<sup>1</sup> Omer Adler,<sup>1</sup> Zahi Hakim,<sup>1</sup> Sabina Pozzi,<sup>3</sup> Anna Scomparin,<sup>3,4</sup> Jonathan Cohen,<sup>5</sup> Muhammad Yassin,<sup>1</sup> Lea Monteran,<sup>1</sup> Rachel Grossman,<sup>6</sup> Galia Tsarfaty,<sup>7</sup> Chen Luxenburg,<sup>5</sup> Ronit Satchi-Fainaro,<sup>3</sup> Tobias Pukrop,<sup>2</sup> and Neta Erez<sup>1,9,\*</sup>

<sup>1</sup>Department of Pathology, Sackler Faculty of Medicine, Tel Aviv University, Tel Aviv 69978, Israel

<sup>2</sup>Department of Internal Medicine III, Hematology and Medical Oncology, University Hospital Regensburg, Regensburg 93053, Germany

<sup>3</sup>Department of Physiology and Pharmacology, Sackler Faculty of Medicine, Tel Aviv University, Tel Aviv 69978, Israel

<sup>4</sup>Department of Drug Science and Technology, University of Turin, Via P. Giuria 9, 10125 Turin, Italy

<sup>5</sup>Department of Cell and Developmental Biology, Sackler Faculty of Medicine, Tel Aviv University, Tel Aviv 69978, Israel

<sup>6</sup>Department of Neurosurgery, Tel Aviv Medical Center, Sackler Faculty of Medicine, Tel Aviv University, Tel Aviv 69978, Israel

<sup>7</sup>Department of Diagnostic Imaging, Chaim Sheba Medical Center, Sackler Faculty of Medicine, Tel Aviv University, Tel Aviv 69978, Israel

<sup>8</sup>These authors contributed equally

<sup>9</sup>Lead Contact

\*Correspondence: [netaerez@tauex.tau.ac.il](mailto:netaerez@tauex.tau.ac.il)

<https://doi.org/10.1016/j.celrep.2019.07.033>

## SUMMARY

Melanoma is the deadliest skin cancer due to its high rate of metastasis, frequently to the brain. Brain metastases are incurable; therefore, understanding melanoma brain metastasis is of great clinical importance. We used a mouse model of spontaneous melanoma brain metastasis to study the interactions of melanomas with the brain microenvironment. We find that CXCL10 is upregulated in metastasis-associated astrocytes in mice and humans and is functionally important for the chemoattraction of melanoma cells. Moreover, CXCR3, the receptor for CXCL10, is upregulated in brain-tropic melanoma cells. Targeting melanoma expression of CXCR3 by nanoparticle-mediated siRNA delivery or by shRNA transduction inhibits melanoma cell migration and attenuates brain metastasis *in vivo*. These findings suggest that the instigation of pro-inflammatory signaling in astrocytes is hijacked by brain-metastasizing tumor cells to promote their metastatic capacity and that the CXCL10-CXCR3 axis may be a potential therapeutic target for the prevention of melanoma brain metastasis.

## INTRODUCTION

Malignant melanoma is the deadliest of all skin cancers (Ankeny et al., 2018; Arnold et al., 2014). The major cause of melanoma mortality is its high metastasis rate to distant organs, frequently to the brain (Nayak et al., 2012). Brain metastases are incurable and are associated with a dismal survival. The incidence of brain metastasis has increased in recent years as a result of improved diagnostic imaging of smaller, asymptomatic brain metastases and improved control of extracranial disease by systemic ther-

apy, enabling the emergence of otherwise not clinically manifested metastases (Nayak et al., 2012; Wang et al., 2017).

Metastasis is a multistage process, facilitated by the microenvironment (Joyce and Pollard, 2009). Multiple studies have demonstrated that changes in the metastatic microenvironment precede clinically relevant metastases (Erez and Coussens, 2011; Joyce and Pollard, 2009; Peinado et al., 2017). Tumor cells were shown to induce the reprogramming of cells in the microenvironment to form a hospitable metastatic niche by paracrine and systemic secretion of soluble factors and exosomes (Hoshino et al., 2015; Peinado et al., 2011, 2017). However, changes in the brain microenvironment that enable metastatic seeding and growth are poorly understood.

The brain encompasses a unique microenvironment that maintains the physiological homeostasis and orchestrates the response to pathological dysregulations, including cancer (Valiente et al., 2018). One of the central components of the brain microenvironment are astrocytes, glial cells that perform many functions in maintaining brain homeostasis and that play a principal role in tissue repair processes. Following brain insult, astrocytes are activated in a response called astrogliosis, characterized by the upregulation of glial fibrillary acidic protein (GFAP), increased production and remodeling of intermediate filament proteins (Pekny et al., 2014), and upregulation of pro-inflammatory cytokines and chemokines (Doron et al., 2019). Astrocyte activation and neuroinflammation can be driven by activated microglia and immune cells (Liddelov and Barres, 2017; Liddelov et al., 2017) and are characterized by the release of pro-inflammatory mediators, increased blood-brain barrier permeability, and leukocyte infiltration (Burda and Sofroniew, 2014). While much data have accumulated on the role of astrogliosis and neuroinflammation in neurodegenerative and autoimmune diseases in the CNS (Skaper et al., 2018), the role of neuroinflammation in brain tropism and metastasis is largely unknown.

Astrocytes were shown to support the growth and infiltration of tumor cells in the brain parenchyma by various mechanisms (Chuang et al., 2013b; Kim et al., 2011; Lin et al., 2010; Placone



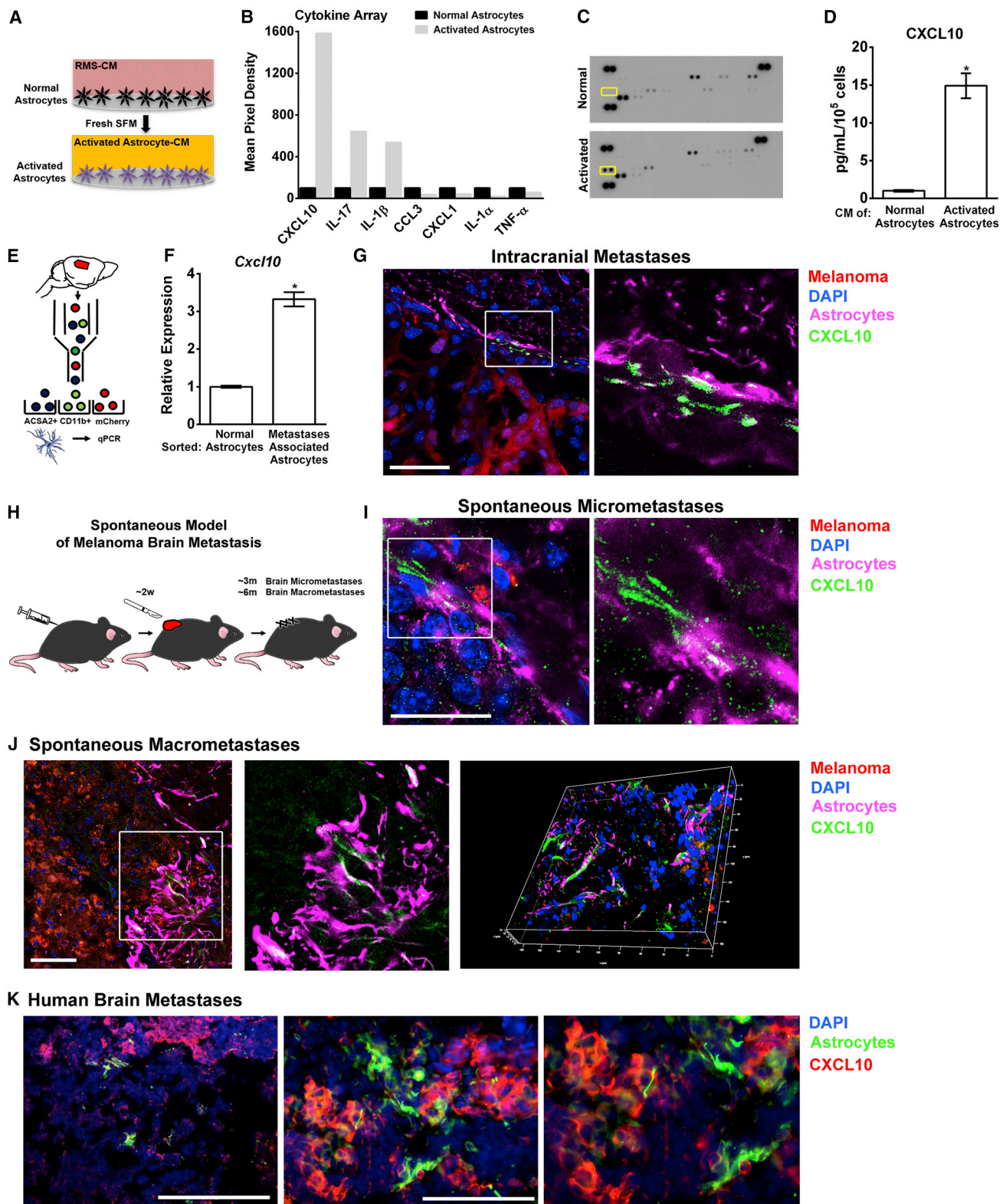


**Figure 1. Astrocytes Are Activated by Melanoma Cells to Express and Secrete Pro-inflammatory Cytokines *In Vitro* and *In Vivo***

(A) Scheme of astrocyte activation: normal astrocytes are incubated with RMS-CM, washed, and incubated with fresh SFM to produce activated astrocyte-CM. SFM, serum-free medium; CM, conditioned medium. Isolation and purity analyses of cultured astrocytes are shown in [Figures S1A–S1E](#).

(legend continued on next page)

et al., 2016). Moreover, astrocytes were implicated in supporting the growth of brain-metastasizing tumor cells via pro-inflammatory signaling (Klein et al., 2015; Priego et al., 2018; Schwartz et al., 2016), but the underlying mechanisms remain unresolved.

We previously established a mouse model of spontaneous melanoma brain metastasis. This model, based on the subdermal implantation of melanoma cells (RMS cells, derived from Ret-melanoma transgenic mice), recapitulates the pathological multistep process of spontaneous metastasis following surgical removal of the primary tumor (Schwartz et al., 2016). We found that astrogliosis and neuroinflammation are instigated during the formation of brain micrometastases and that astrocytes facilitate the initial growth of melanoma cells in the brain. Furthermore, we showed that the chemokine CXCL10, known to be upregulated during gliosis (Zamanian et al., 2012), is upregulated in the brain metastatic microenvironment. CXCL10 belongs to the CXC chemokine family and is a ligand of the CXCR3 receptor. CXCL10 is secreted in response to interferon- $\gamma$  (IFN- $\gamma$ ) by various cell types, including monocytes, endothelial cells, fibroblasts, and astrocytes, and was shown to modulate the migration of monocytes, macrophages, T cells, and natural killer (NK) cells (Metzemaekers et al., 2018). Moreover, CXCL10 levels are elevated in advanced melanoma patients and were associated with poor clinical outcomes (Jiang et al., 2015; Wightman et al., 2015). We therefore hypothesized that astrocyte-derived CXCL10 may be involved in facilitating melanoma brain tropism and metastasis.

Here, we show that the chemokine CXCL10 is upregulated in metastases-associated astrocytes, and its secretion is functionally important for the astrocyte-mediated chemoattraction of melanoma cells. Moreover, we found that the CXCL10 receptor CXCR3 is upregulated in brain-tropic melanoma cells, and that targeting its expression resulted in the inhibition of melanoma brain metastasis.

## RESULTS

### CXCL10 Is Upregulated in Metastasis-Associated Astrocytes

We previously demonstrated that astrocytes are activated by melanoma-secreted factors to upregulate the expression of mul-

iple pro-inflammatory factors, including CXCL10 (Schwartz et al., 2016). To investigate pro-inflammatory reprogramming of astrocytes by melanoma cells, we performed experiments with primary astrocytes, isolated from normal adult mice (Figure S1A). Analysis of cultured astrocytes by immunostaining, qPCR, and fluorescence-activated cell sorting (FACS) confirmed the purity of isolated astrocytes. Astrocyte cultures did not contain immune cells or microglia (Figures S1B–S1E). We then analyzed the expression of multiple inflammatory mediators in astrocytes activated by incubation with melanoma-secreted factors using a cytokine array. We found that CXCL10 was the most highly upregulated factor in activated astrocytes (Figures 1A–1C). Control non-activated astrocytes had almost no basal CXCL10 expression, in agreement with our previous observations at the mRNA level (Schwartz et al., 2016). Analysis of CXCL10 secretion by ELISA confirmed that CXCL10 was highly secreted by activated astrocytes compared to normal astrocytes (Figure 1D). We next set out to assess whether CXCL10 is expressed in metastases-associated astrocytes (MAAs) *in vivo*. To that end, we isolated MAAs by FACS sorting of mCherry<sup>-</sup>CD45<sup>-</sup>ACSA-2<sup>+</sup> cells from the brains of mice bearing macrometastases from intracardiac or intracranial injections (Figures 1E and S1F). The purity of sorted astrocytes was validated by analyzing the expression of cell-specific markers (Figure S1G). Expression analysis of sorted cells revealed that *Cxcl10* was highly upregulated in MAAs compared with normal astrocytes (Figure 1F). To further validate the expression of CXCL10 in MAAs *in vivo*, we performed co-staining of CXCL10 and GFAP in melanoma lesions arising in the brains of mice that were injected intracranially, as compared with normal brains. Analysis of the results revealed that reactive astrocytes adjacent to melanoma cells expressed CXCL10 (Figures 1G, S2A, and S2B). We also validated the expression of CXCL10 in MAAs in our established model of spontaneous brain metastasis (Figure 1H). Brains bearing spontaneous metastases showed CXCL10 expression in astrocytes already in micrometastases (Figures 1I, S2C, and S2D). The expression of CXCL10 was evident also in MAAs adjacent to spontaneous macrometastases (Figure 1J), suggesting that CXCL10 plays a role throughout different stages of metastasis formation. Notably, while CXCL10

(B and C) Cytokine array analysis (B) and representative membrane blots (C) of pro-inflammatory factors in activated astrocytes and normal astrocytes. Astrocytes were activated as in (A), lysed, and hybridized with the mouse cytokine array panel. In (C), box indicates CXCL10; n = 2.

(D) ELISA of CXCL10 in normal or activated astrocyte-CM, representative of n = 3 independent experiments. The data are presented as means  $\pm$  SDs of technical duplicates; one-tailed Student's t test; \*p = 0.0260.

(E) Sorting strategy for metastases-associated astrocytes. The ACSA-2 antibody was used to isolate astrocytes from normal brains or macrometastases-bearing brains following intracardiac or intracranial injections. The purity analysis of sorted astrocytes is shown in Figures S1F and S1G.

(F) *Cxcl10* expression was analyzed by qPCR and the results were normalized to *Hprt* and to the normal control group. Representative of n = 2 independent experiments, n = 4 pooled brains in each. The data are presented as means  $\pm$  SDs of technical repeats; two-tailed Student's t test; \*p = 0.0329.

(G) Co-staining of astrocytes (GFAP, magenta) and CXCL10 (green) in brain macrometastases following intracranial injections (melanoma, mCherry red). Scale bar, 50  $\mu$ m. At right, only the magenta and green channels are shown.

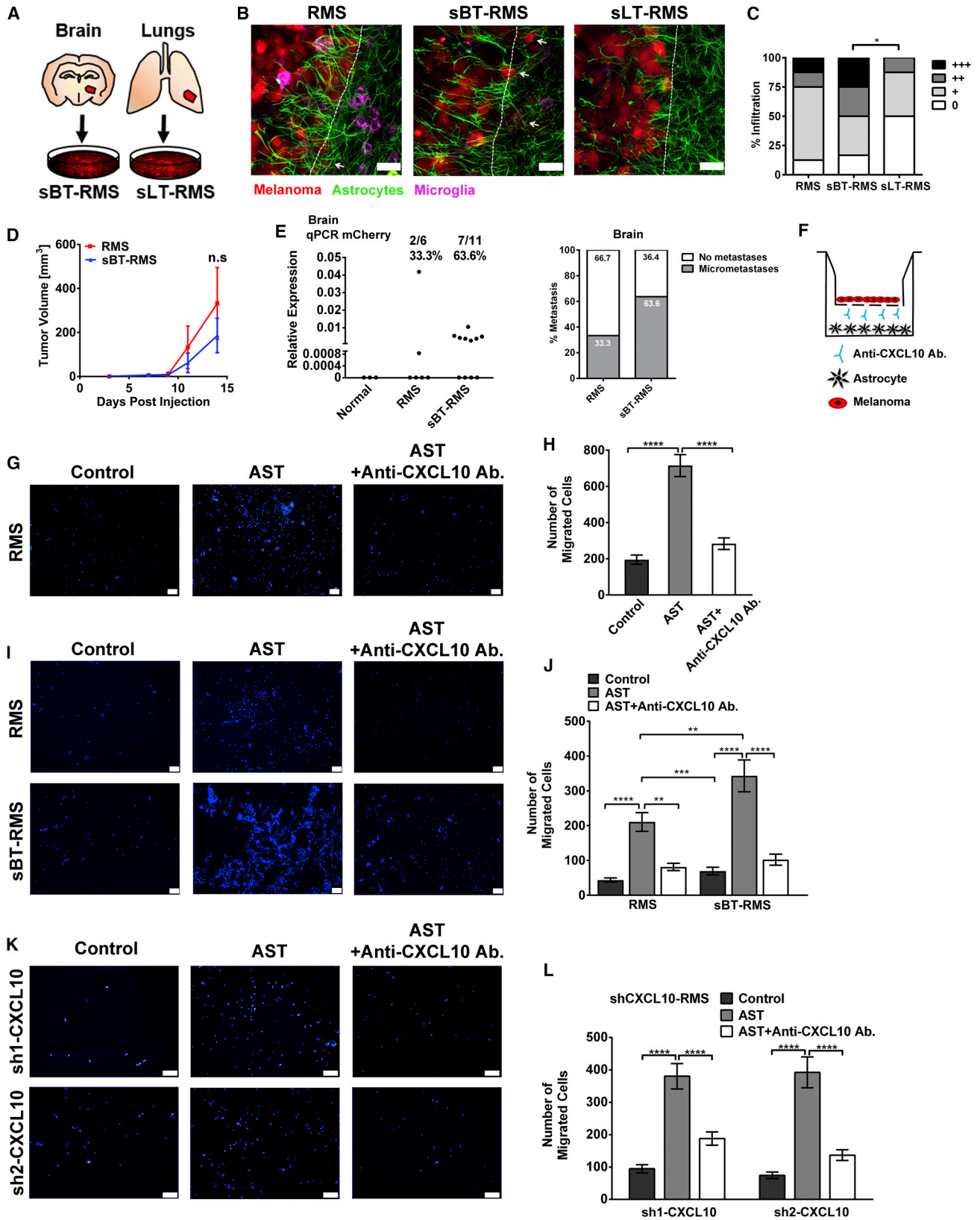
(H) Spontaneous melanoma brain metastasis model scheme.

(I) Co-staining of astrocytes (GFAP, magenta) and CXCL10 (green) in spontaneous brain micrometastases (melanoma, mCherry red). Scale bar, 25  $\mu$ m. At right, only the magenta and green channels are shown.

(J) Co-staining of astrocytes (GFAP, magenta) and CXCL10 (green) in spontaneous brain macrometastases (melanoma, mCherry red). Scale bar, 50  $\mu$ m. Only the magenta and green channels are shown in the center. The 3D maximal projection is shown at right.

(K) Co-staining of astrocytes (GFAP, green) and CXCL10 (red) in human tissue sections of melanoma brain metastases. Left: scale bar represents 400  $\mu$ m. Center: scale bar represents 100  $\mu$ m. Right: digital enlargement of center image. Representative of multiple fields analyzed from n = 2 patients.

(G–J) White, colocalization of astrocytes (magenta) with CXCL10 (green). At right in (G) and (I) and center in (J) digital enlargement of areas designated with rectangles are shown. The images are representative of multiple fields analyzed from n = 3 mice per group. Additional images are shown in Figures S2A–S2D.



(legend on next page)

and GFAP stainings overlapped, they were not completely aligned, as GFAP is a cytoskeletal marker and CXCL10 is a cytoplasmic or secreted protein (Figure 1J, right panel). Finally, we asked whether CXCL10 expression in astrocytes is relevant to human melanoma brain metastasis. To that end, we analyzed frozen specimens obtained from patients undergoing surgical resection of melanoma brain metastases. Co-staining with GFAP and CXCL10 confirmed that CXCL10 is expressed in astrocytes infiltrating metastatic melanoma lesions (Figure 1K). Similar to our findings in the mouse model, CXCL10 was expressed in human melanoma brain metastatic cells. These results support our findings that CXCL10 expression is characteristic of inflammatory astrocytes in brain metastasis, and it encouraged us to further unravel its functional role.

### CXCL10 Is Functionally Necessary for Astrocyte-Driven Melanoma Cell Migration

CXCL10 is a known T cell chemoattractant, operating via its cognate receptor CXCR3 (Metzemaekers et al., 2018). Astrocytes were recently shown to orchestrate T cell recruitment to the brain via their CXCL10 secretion in multiple sclerosis (Cheng and Chen, 2014; Sørensen et al., 2002) and during viral CNS infections (Phares et al., 2013). We therefore hypothesized that melanoma cells hijack this physiological pathway, resulting in the brain tropism of brain-metastasizing melanoma cells. To test our hypothesis, we characterized the role of astrocyte-derived CXCL10 in mediating the chemoattraction of melanoma cells to the brain. To that end, we established a spontaneous brain-seeking melanoma cell line by injecting mice subdermally with RMS cells. Primary tumors were surgically removed, and melanoma cells from ensuing spontaneous melanoma brain and lung macrometastases were isolated and cultured. These cells were designated sBT-RMS (spontaneous brain-tropic RMS) and sLT-RMS (spontaneous lung-tropic RMS), respectively (Figure 2A). To assess the brain-infiltrating capacity of the metastatic variants, we used an *ex vivo* 3-dimensional (3D) organotypic model that allows the quantification of tumor cell infiltration to the brain parenchyma (Figure S2E; Chuang et al.,

2013a; Schwartz et al., 2016). Analysis of the results revealed that sBT-RMS cells exhibited a higher capacity to infiltrate the brain parenchyma compared with the RMS parental melanoma cell line. This infiltrative capacity was brain specific, as the infiltration of the lung-tropic variant was significantly lower (Figures 2B, 2C, and S2F). To further validate the brain tropism of the newly isolated sBT-RMS cells compared to RMS cells *in vivo*, we injected the cells subdermally. Notably, analysis of primary tumor growth indicated similar growth kinetics (Figure 2D). Analysis of brain metastatic load indicated that sBT-RMS-injected mice developed more brain micrometastases compared with RMS-injected mice (Figure 2E). This advantage was indeed brain specific: analysis of lung metastatic load by gross inspection and by qPCR analysis indicated that sBT-RMS-injected mice had fewer lung macrometastases compared to the RMS-injected group (Figures S2G and S2H). Thus, the establishment of brain tropism following interactions between melanoma cells and the brain microenvironment may be organ specific.

We next assessed the functional role of astrocyte-derived CXCL10 in mediating melanoma cell migration by analyzing the migration of melanoma cells toward astrocytes in Transwell assays. To specifically analyze the functional importance of CXCL10 in promoting melanoma cell migration, we added neutralizing antibodies (Figure 2F). We found that CXCL10 neutralization significantly attenuated melanoma cell migration toward astrocytes, suggesting that astrocyte-induced migration of melanoma cells is mediated, at least partially, by CXCL10 (Figures 2G and 2H).

Intrigued by these findings, we asked whether the brain-tropic nature of the sBT-RMS cell line is dependent on CXCL10. To that end, we tested the migration capacity of the sBT-RMS cell line toward astrocytes as compared with RMS cells. We found that both RMS and sBT-RMS cells exhibited increased migration toward astrocytes compared to the serum-free media (SFM) control and that sBT-RMS cells had a significantly enhanced capacity to migrate toward astrocytes. This effect was inhibited by the addition of CXCL10-neutralizing antibodies (Figures 2I and 2J). Thus, the enhanced brain-metastatic capacity of the sBT-RMS

### Figure 2. Astrocyte-Derived CXCL10 Facilitates Melanoma Cell Migration

(A) Illustration of sBT-RMS and sLT-RMS cell isolation.

(B) Representative images of the organotypic co-culture with RMS, sBT-RMS, and sLT-RMS cell lines infiltrating the brain slice and astrocytes protruding into tumor plugs. Scale bars, 30  $\mu$ m. Melanoma cells (mCherry, red), astrocytes (GFAP, green), and microglia (isolectin B4 [ILB4], magenta). Experiment scheme and corresponding lower magnifications shown in Figures S2E and S2F.

(C) Quantification of the relative infiltration of the different cell lines. RMS: n = 16, sBT-RMS: n = 26, sLT-RMS: n = 15. Chi-square test, \*p = 0.02.

(D and E) Analysis of sBT-RMS brain-metastatic potential *in vivo*, compared to parental RMS cells, using the spontaneous model shown in Figure 1H. n = 12 mice per group were injected and excluded from analysis if lung macrometastases or primary tumor recurrences formed before the endpoint. (D) Primary tumor growth kinetics of RMS or sBT-RMS-injected mice. The data are presented as means  $\pm$  SEMs; n.s., not significant. (E) qPCR analysis of mCherry expression as a determinant of brain metastatic load, showing the percentage of mice with brain micrometastases. RMS: n = 6, sBT-RMS: n = 11, normal controls: n = 3. The analysis of the lung metastasis is shown in Figures S2G and S2H.

(F) Transwell assay experimental design, 48 h migration.

(G) Representative images of RMS migration toward control (SFM), astrocytes (AST), or astrocytes +anti-CXCL10 antibody (Ab.); scale bars, 500  $\mu$ m.

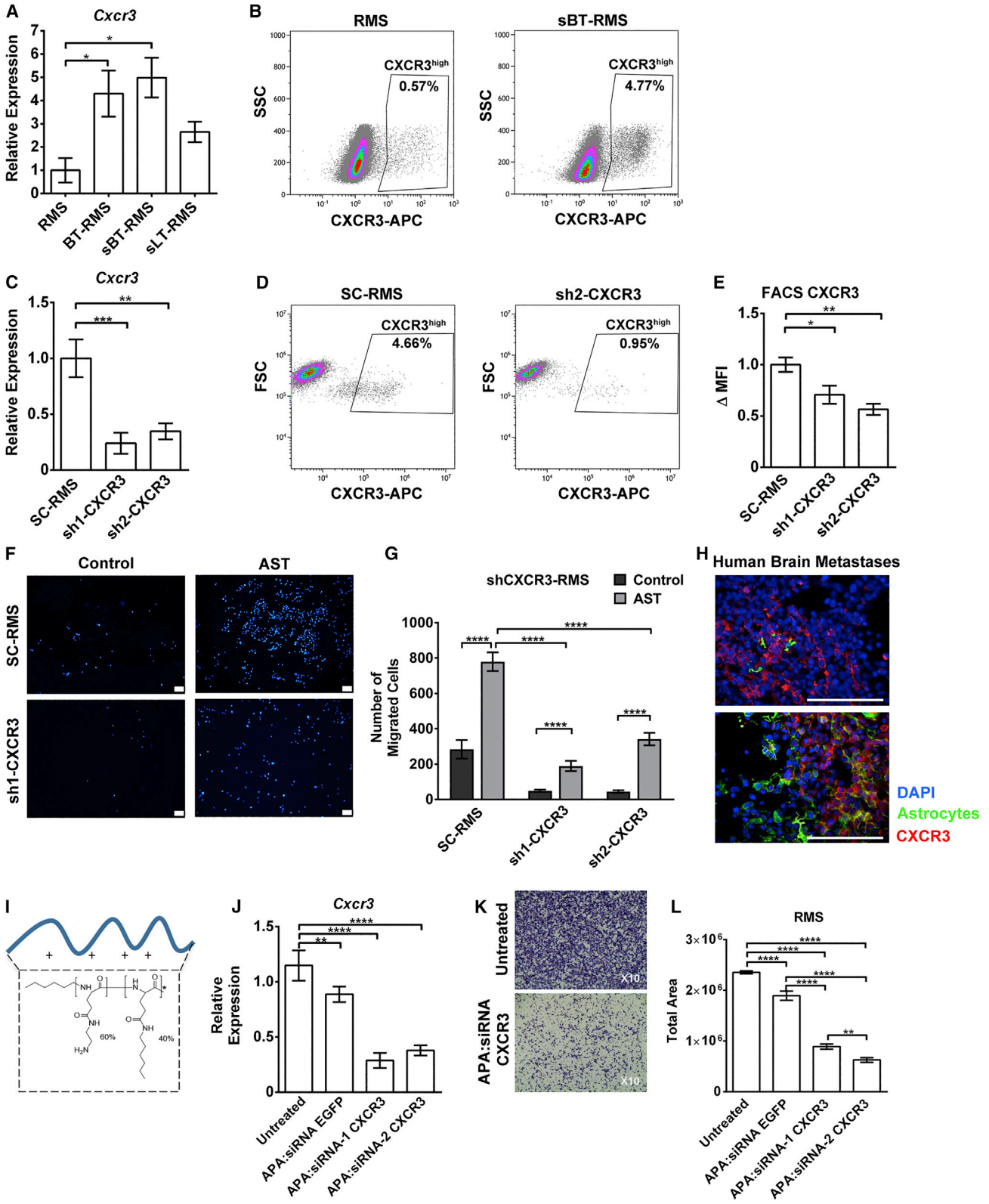
(H) Quantification of (G); the data are presented as means  $\pm$  SEMs of 45 fields per treatment group from n = 3 independent biological repeats. One-way ANOVA with Tukey's post hoc test; \*\*\*\*p < 0.0001.

(I) Representative images of RMS and sBT-RMS migration toward SFM, astrocytes, or astrocytes +anti-CXCL10 Ab.; scale bars, 500  $\mu$ m.

(J) Quantification of (I); the data are presented as means  $\pm$  SEMs of 30 fields per treatment group from n = 3 independent biological repeats. Two-way ANOVA with Tukey's post hoc test; \*\*p < 0.002, \*\*\*p < 0.0005, and \*\*\*\*p < 0.0001.

(K) Representative images of sh1-CXCL10 and sh2-CXCL10 migration toward SFM, astrocytes, and astrocytes +anti-CXCL10 Ab.; scale bars, 150  $\mu$ m.

(L) Quantification of (K); the data are presented as means  $\pm$  SEMs of 30 fields per treatment group from n = 3 independent biological repeats. Two-way ANOVA with Tukey's post hoc test; \*\*\*\*p < 0.0001. CXCL10 silencing validation and the scramble control migration experiment are shown in Figures S2I and S2J.



(legend on next page)

cells may be mediated by astrocyte-derived CXCL10 signaling. Since melanoma cells also express CXCL10 (Harlin et al., 2009; Mauldin et al., 2015), we wanted to specifically analyze the functional importance of astrocyte-derived CXCL10 for melanoma cell migration. To that end, we knocked down the expression of CXCL10 in melanoma cells by lentiviral transduction of CXCL10-targeting small hairpin RNA (shRNA), so that astrocytes are the only source of CXCL10 in the Transwell migration assays. CXCL10 knockdown (KD) was confirmed by qPCR analysis of the CXCL10-KD variants (sh1- and sh2-CXCL10 RMS cells) compared to the scramble-infected (SC-RMS) control cells (Figure S2I). Transwell migration assays indicated that inhibiting the function of astrocyte-derived CXCL10 with neutralizing antibodies significantly attenuated tumor cell migration (Figures 2K and 2L), further confirming the central role of astrocyte-derived CXCL10. SC-RMS cells had a higher overall migration compared with CXCL10-KD cells (Figure S2J), demonstrating the role of autocrine CXCL10 signaling in enhancing the migration of melanoma cells. Thus, while melanoma autocrine CXCL10 signaling can mediate cell migration, we show that astrocyte-derived CXCL10 is functionally important in enhancing melanoma migration.

### CXCR3 Is Highly Expressed in Brain-Tropic Melanoma Cells and Is Functionally Important in Facilitating Melanoma Cell Migration

The CXCL10-CXCR3 axis was previously shown to be involved in the tropism of melanoma cells to the lungs (Wightman et al., 2015). However, the role of astrocyte-derived CXCL10 in facilitating brain tropism via this signaling axis is unknown. Thus, we compared CXCR3 expression in the parental cell line (RMS) with organ-tropic variants, including a brain-tropic variant (BT-RMS) that we previously established by serial intracardiac injections (Schwartz et al., 2016), and the spontaneous brain-tropic and lung-tropic melanoma cells (sBT-RMS and sLT-RMS,

respectively). qPCR analysis revealed that the brain-tropic variants of melanoma expressed higher levels of *Cxcr3* compared to the parental cells (Figure 3A). Analysis at the protein level by FACS confirmed that a subpopulation of sBT-RMS cells express higher levels of CXCR3 compared to RMS (Figures 3B and S3A). Thus, CXCR3 is upregulated in brain-tropic cells, suggesting that this chemokine receptor has a functional role in the capacity of melanoma cells to metastasize to the brain. To investigate the functional role of CXCR3 in melanoma brain tropism, we knocked down its expression by lentiviral transduction in RMS cells. Analysis of knockdown efficacy at the RNA level confirmed a significant silencing of *Cxcr3* expression (Figure 3C), and FACS analysis verified the downregulation of CXCR3 (Figures 3D, 3E, and S3B), providing us with an experimental tool to further study the functional role of CXCR3 in mediating melanoma cell migration and brain metastasis. We next performed a migration assay and found that the migration of CXCR3-KD RMS cells toward astrocytes was strongly attenuated compared to the SC-RMS control (Figures 3F and 3G), confirming that melanoma cell migration is mediated by the CXCL10-CXCR3 axis. Immunostaining of tissue samples from patients with melanoma brain metastases showed that CXCR3 is expressed in human brain metastatic melanoma cells, suggesting that this signaling axis plays a role in human disease (Figure 3H).

Based on these findings, we next asked whether CXCR3 could be a potential therapeutic target to inhibit melanoma migration and metastasis. For therapeutic targeting, we used amphiphilic polyplex nanocarriers, which were recently shown to be effective for the systemic administration of RNAi to tumors (Krivitsky et al., 2018; Polyak et al., 2017). Moreover, the amphiphilic polyglutamate amine (APA) polymeric nanocarrier complexed with a combination of miR-34a and small interfering RNA (siRNA) targeting PLK1 was demonstrated to be therapeutically functional in a mouse model of orthotopic pancreatic cancer by inhibiting tumor growth and prolonging survival (Gibori et al., 2018). Here, we

### Figure 3. CXCR3 Is Highly Expressed in Brain-Tropic Melanoma Cells and Is Functionally Important for Melanoma Cell Migration

- (A) qPCR analysis of *Cxcr3* in the different RMS variants *in vitro*. The results were normalized to Hprt and RMS. The data are presented as means  $\pm$  SEMs from  $n = 3$  independent repeats. One-way ANOVA with Tukey's post hoc test; \* $p = 0.0267$ .
- (B) FACS analysis of CXCR3 in cultured RMS and sBT-RMS cells. Representative of  $n = 3$  independent repeats. Isotype control and gating strategy are shown in Figure S3A. SSC, side scatter.
- (C) qPCR analysis of *Cxcr3* silencing validation in the CXCR3-KD cell lines. The results were normalized to Hprt and SC-RMS. The data are presented as means  $\pm$  SEMs of the biological repeats from  $n = 5$  experiments. One-way ANOVA with Tukey's post hoc test; \*\* $p = 0.0024$  and \*\*\* $p = 0.0003$ .
- (D) FACS analysis of CXCR3 expression in cultured SC-RMS and sh2-CXCR3 cells. Representative of  $n = 2$  repeats. Isotype control and gating strategy are shown in Figure S3B. FSC, forward scatter.
- (E) CXCR3 expression in the total cell population presented as a quantification of mean fluorescent intensity ( $\Delta$ MFI). The data are presented as means  $\pm$  SEMs of the measurements from  $n = 2$  independent repeats. The results were normalized to SC-RMS. One-way ANOVA with Tukey's post hoc test; \* $p = 0.0322$  and \*\* $p = 0.0024$ .
- (F) Representative images of sh1-CXCR3 and sh2-CXCR3 migration toward SFM and astrocytes, seeded and analyzed as in Figure 2F. Scale bars, 500  $\mu$ m.
- (G) Quantification of (F). The data are presented as means  $\pm$  SEMs of 30 fields from  $n = 3$  independent repeats. Two-way ANOVA with Tukey's post hoc test; \*\*\*\* $p < 0.0001$ .
- (H) Co-staining of astrocytes (GFAP, green) and CXCR3 (red) in human tissue sections of melanoma brain metastases. Scale bars, 100  $\mu$ m. Representative of multiple fields analyzed from  $n = 2$  patients.
- (I) Scheme of the amphiphilic aminated poly( $\alpha$ )glutamate cationic-based polymer (APA).
- (J) Representative qPCR analysis of *Cxcr3* in RMS cells incubated with polyplexes APA:siRNA-1 CXCR3 or APA:siRNA-2 CXCR3 compared to untreated or negative control siRNA (APA:siRNA EGFP). The results were normalized to Hprt and the untreated control. The data are presented as means  $\pm$  SDs of technical repeats;  $n = 2$  independent repeats. One-way ANOVA with Tukey's post hoc test; \*\* $p = 0.003$  and \*\*\*\* $p < 0.0001$ .
- (K) Representative migration images of RMS cells treated with the polyplex targeting CXCR3, at 10 $\times$  magnification.
- (L) Quantification of (K). The data are presented as means  $\pm$  SEMs of the technical repeats from  $n = 2$  independent experiments. One-way ANOVA with Tukey's post hoc test; \*\* $p = 0.0042$  and \*\*\*\* $p < 0.0001$ . Additional data on the polyplexes are presented in Figures S3C and S3D.

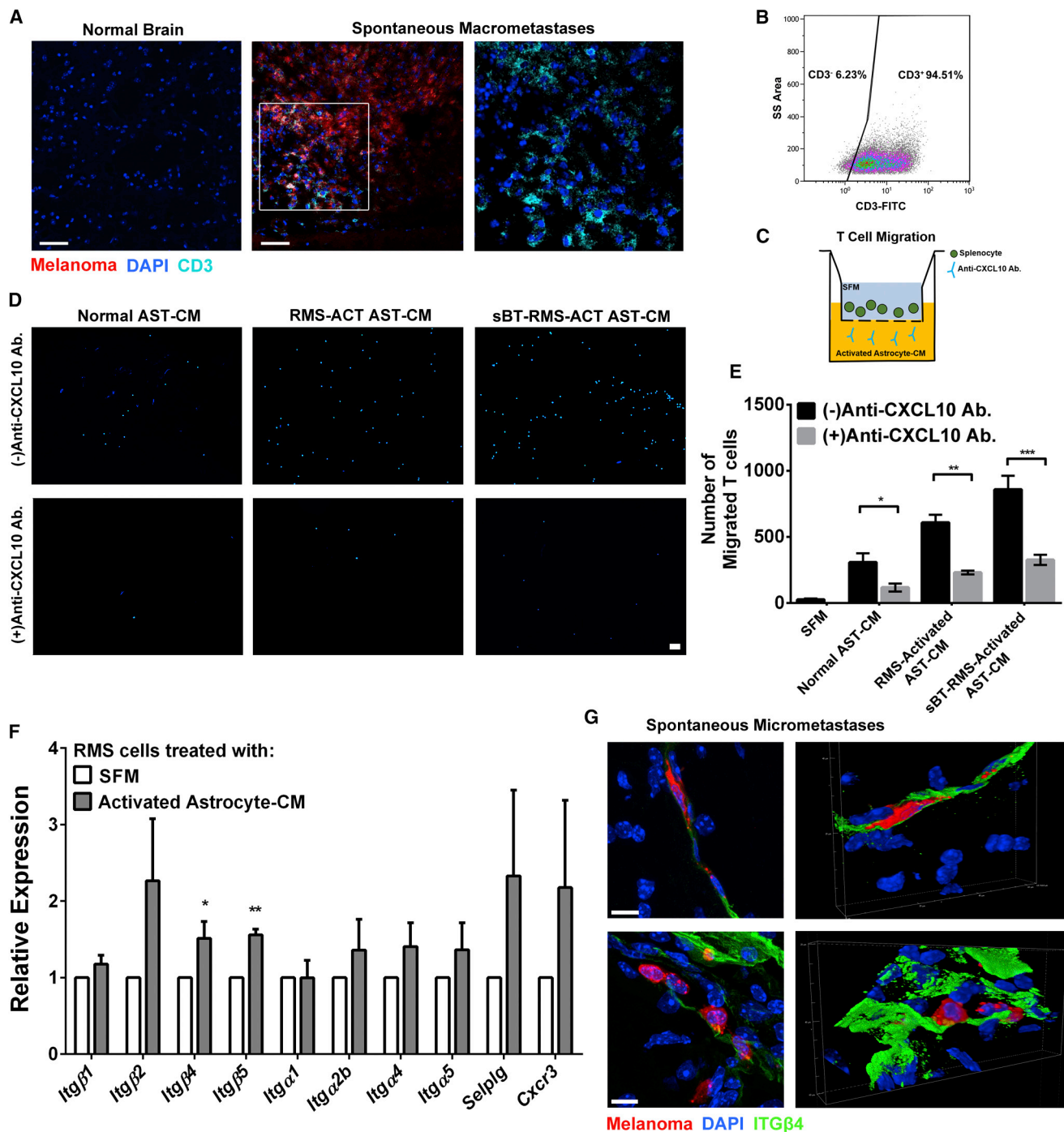


**Figure 4. T Cell Migration Is Facilitated by Astrocyte-Derived CXCL10**

(A) T cell (CD3, cyan) staining in normal brain or spontaneous brain macrometastases (melanoma, mCherry red). Scale bars, 50  $\mu$ m. Representative images from multiple fields analyzed in  $n = 2$  mice. The white rectangle designates the digital enlarged area shown at right. Right, overlay of the cyan and blue channels.

(B) Purity FACS analysis of cultured splenocytes, using CD3-FITC (fluorescein isothiocyanate) antibody.

(C) Experimental design for T cell migration. The lower chamber contained SFM, normal astrocyte-CM, or CM of astrocytes activated by RMS or sBT-RMS-CM. Migration was assessed after incubation for 5 h.

(D) Representative images of T cell migration described in (C); scale bar, 200  $\mu$ m.

(E) Quantification of migrated T cells shown in (D). The data are presented as means  $\pm$  SEMs of six fields from  $n = 3$  independent repeats. Multiple two-tailed t test analysis; \* $p = 0.042$ , \*\* $p < 0.00001$ , and \*\*\* $p < 0.000001$ .

(F and G) Activated astrocyte soluble factors upregulate integrins in melanoma cells.

(legend continued on next page)

complexed APA with RNAi to silence *Cxcr3*. Two sequences of siRNA oligonucleotide sequences targeting *Cxcr3* (siRNA-1 and siRNA-2) were used for the complexation with APA (Figure 3I). Electrophoretic mobility shift assay (EMSA) verified the formation of the polymer:siRNA polyplexes according to the number of positively charged amino groups (N) neutralized by the negative charge of the siRNA phosphates (P). The selected N:P ratio 2, resulted in nanosized (~180 nm) and positively charged ( $\zeta$  potential of ~+22 mV) polyplexes. The obtained polyplex is stable for up to 24 h in plasma, protecting the siRNA from degradation in the bloodstream (Figure S3C). Both APA:CXCR3 siRNA-1 and siRNA-2 polyplexes significantly reduced the expression of *Cxcr3* compared to the untreated and the negative control (NC) siRNAs (Figure 3J). Furthermore, the APA:CXCR3-siRNA polyplexes did not show toxic effects on the viability of melanoma cells (Figure S3D). The achieved downregulation of *Cxcr3* resulted in a significant inhibition (60%–70%) of melanoma cell migration toward astrocytes, compared to the migration of untreated cells (Figures 3K and 3L), suggesting that targeting CXCR3 on tumor cells may be therapeutically beneficial. To further elucidate the importance of CXCR3 in facilitating brain tropism, we engineered the parental RMS cells to overexpress CXCR3 (Figure S4A) and tested the effect of this enhanced expression on their capacity to colonize the brain, as compared with control cells transduced with the backbone plasmid. Analysis of brain metastases indicated that CXCR3-overexpressing RMS cells formed more brain macrometastases (Figures S4C and S4D). sLT cells did not form any brain macrometastases, even following the overexpression of CXCR3 (Figures S4B and S4C), suggesting that their reprogramming in the lung microenvironment was organ specific, and did not endow them with an advantage in the brain. These results support our hypothesis that CXCR3<sup>high</sup> melanoma cells are better equipped to colonize the brain.

### CXCL10 Secreted from Melanoma-Activated Astrocytes Enhances T Cell Migration and Upregulates ITG $\beta$ 4 in Melanoma Cells

Previous studies demonstrated the presence of T cells in human melanoma brain metastasis (Amit et al., 2013; Berghoff et al., 2015b). To assess T cell infiltration to melanoma brain metastasis, we performed immunostaining, which indicated that CD3<sup>+</sup> T cells were associated with spontaneous melanoma brain macrometastases, but they could not be detected in normal brains (Figure 4A). Since CXCL10 is a known chemoattractant for T cells, we next asked whether pro-inflammatory activation of astrocytes by melanoma cells facilitates their capacity to recruit T cells. We isolated murine splenocytes and validated their purity (Figure 4B). We then assessed the capacity of T cells to migrate toward astrocyte-secreted factors using a Transwell assay (Figure 4C). T cell migration toward activated astrocyte-CM (conditioned medium) (activation as in Figure 1A) was

enhanced compared to their migration toward normal astrocyte-CM. Moreover, the activation of astrocytes by secreted factors of brain-tropic cells (sBT-RMS-CM) gave rise to significantly more T cell migration than normal astrocyte-CM, suggesting that the interactions of astrocytes with melanoma cells activate their physiological tissue damage response, resulting in the instigation of neuroinflammation. Furthermore, the addition of CXCL10-neutralizing antibodies significantly inhibited T cell migration (Figures 4D and 4E), suggesting that astrocyte-derived CXCL10 is necessary for mediating T cell chemoattraction, in agreement with its physiological role.

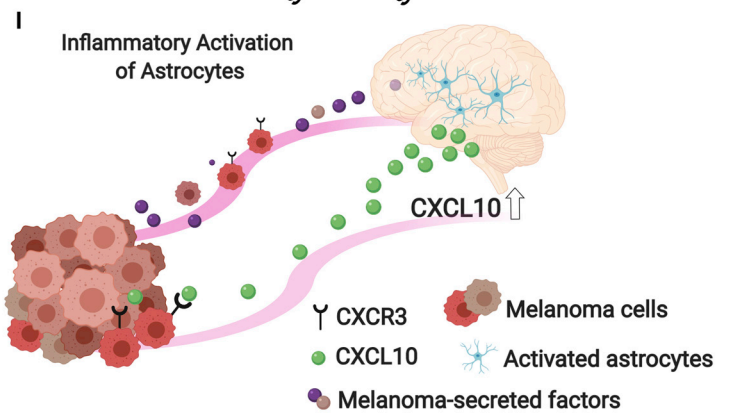
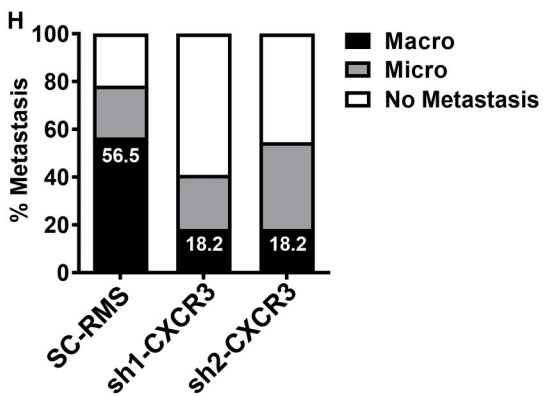
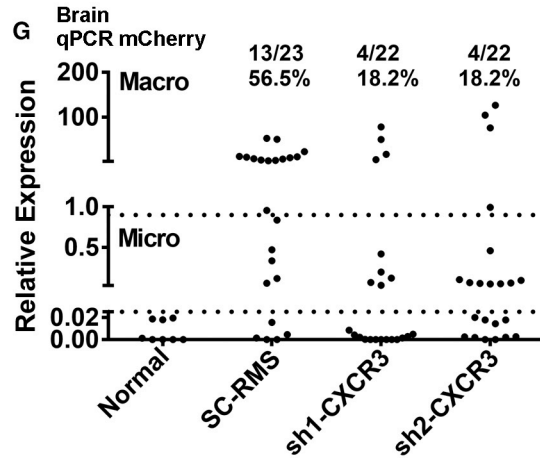
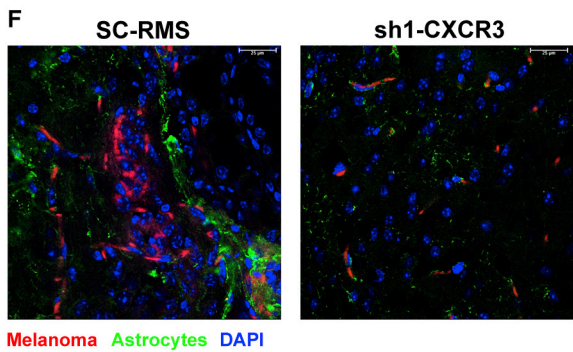
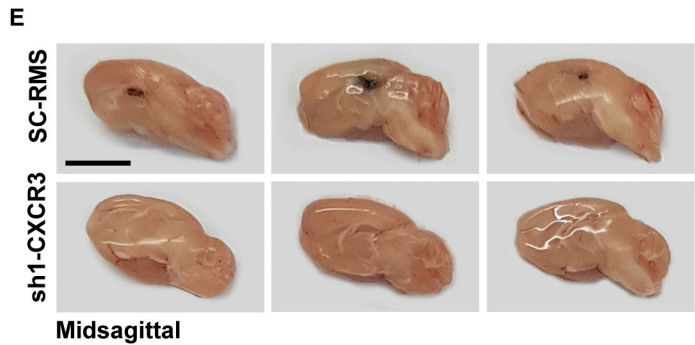
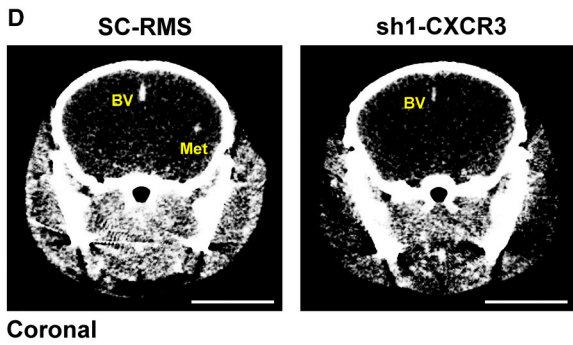
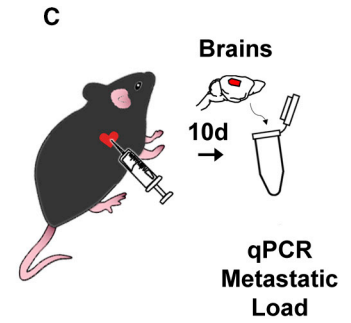
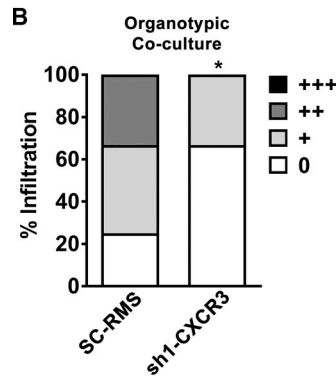
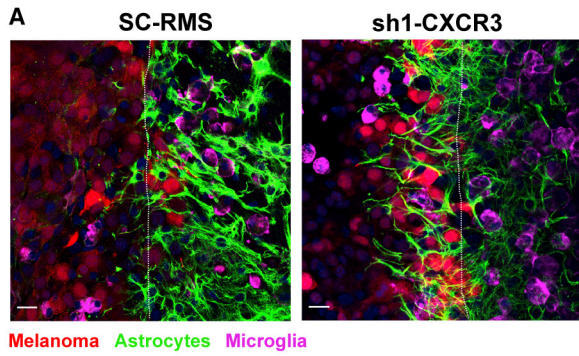
Adhesion molecules were previously shown to participate in the homing and infiltration of T cells into the brain (Baron et al., 1993; Denucci et al., 2009; Engelhardt and Ransohoff, 2005). We hypothesized that these signaling pathways may be hijacked to facilitate melanoma cell adhesion in the brain. To test this hypothesis and gain mechanistic insights on CXCR3-driven signaling in promoting brain tropism, we analyzed whether astrocyte-derived factors affected the expression of known adhesion molecules in melanoma cells. Incubation of melanoma cells with astrocyte-CM upregulated *Cxcr3*, *Itg $\beta$ 2* (*Lfa-1*), *Itg $\beta$ 4*, *Itg $\beta$ 5*, and *Selpg* levels (Figure 4F). To assess whether integrin upregulation could be downstream of CXCR3, we incubated CXCR3-overexpressing RMS cells with activated astrocyte-CM. Analysis of the results revealed an upregulation of *Itg $\beta$ 4* and *Itg $\alpha$ 1* in CXCR3-overexpressing RMS cells, compared to the parental RMS cells (Figure S5A). Notably, integrin  $\beta$ 4 (ITG $\beta$ 4) and ITG $\beta$ 5 were recently shown to be expressed in brain organotypic melanoma cells and exosomes and to mediate breast cancer lung and liver metastases (Hoshino et al., 2015). We therefore tested whether ITG $\beta$ 4 is evident in early brain metastasis. Staining of spontaneous brain micrometastases specimens indicated that ITG $\beta$ 4 was expressed by metastasizing melanoma cells and by the associated blood vessels, but not in normal brains (Figures 4G, S5B, and S5C). These results suggest that the physiological function of astrocytes in T cell recruitment is hijacked by melanoma cells via the upregulation of adhesion molecules in brain-metastasizing melanoma cells.

### CXCR3 Is Functionally Important for the Formation of Melanoma Brain Metastases *In Vivo*

Encouraged by the *in vitro* results, we next investigated the role of CXCR3 in facilitating brain tropism *in vivo*. Analysis of CXCR3-KD cell infiltration in the organotypic *ex vivo* 3D system demonstrated that targeting the expression of CXCR3 in melanoma cells significantly inhibited their capacity to infiltrate brain tissue, as compared with control cells, suggesting that CXCR3 is an important mediator of brain colonization (Figures 5A and 5B). Finally, we investigated the functional importance of CXCR3 in melanoma brain tropism by analyzing the formation of experimental brain metastasis following the intracardiac injection of CXCR3-KD RMS or SC-RMS control cells (Figure 5C). The early

(F) qPCR analysis of integrin expression in RMS cells following incubation for 48 h with activated astrocyte-CM. The results were normalized to *Hprt* and the SFM control of each independent repeat (fold change). The data are presented as means  $\pm$  SEMs of  $n = 3$  independent experiments, one-tailed *t* test; \* $p = 0.0397$  and \*\* $p = 0.0009$ . A similar experiment with CXCR3-overexpressing cells is shown in Figure S5A.

(G) Staining of spontaneous brain micrometastases (melanoma, mCherry red) with ITG $\beta$ 4 (green); 2D and 3D maximal projections. Scale bars, 10  $\mu$ m. Multiple fields analyzed from  $n = 3$  mice. Additional images are shown in Figure S5B.



(legend on next page)

formation of macrometastases was assessed by intravital computed tomography (CT) imaging 9 days after injections, which indicated that mice injected with CXCR3-KD RMS cells had fewer metastatic lesions (Figures 5D, S5D, and S5E). Mice were euthanized the next day, and the gross inspection of brains confirmed that the inhibition of CXCR3 resulted in fewer macrometastases (Figure 5E). Moreover, we histologically validated the presence of metastases and found that SC-RMS cells formed larger metastatic lesions, which were associated with extensive astrogliosis (Figure 5F). Quantitative analysis of brain metastatic load by qPCR for mCherry was consistent with the macroscopic observations: CXCR3 knockdown decreased the occurrence of brain macrometastases by ~38%. While 56.5% of SC-RMS-injected mice developed brain macrometastases, only 18.2% of the mice injected with CXCR3-KD melanoma cells exhibited macrometastatic lesions (Figures 5G and 5H). Our results implicate the CXCL10-CXCR3 axis in mediating the brain tropism of melanoma cells via interactions with astrocytes (Figure 5I).

## DISCUSSION

The formation of a hospitable metastatic niche, providing a growth-promoting environment for metastasizing tumor cells, is one of the determinants of organ-specific tropism. Astrocytes are major players in mediating neuroinflammation (Skaper et al., 2018), but their role in facilitating the formation of brain metastases is largely unknown. Here, we show that astrocyte-mediated inflammatory signaling via the CXCL10-CXCR3 axis is functionally important for promoting the brain tropism of melanoma.

We demonstrated that melanoma-secreted factors instigate the pro-inflammatory reprogramming of normal astrocytes and the upregulation of multiple pro-inflammatory mediators, including CXCL10. This pro-inflammatory gene signature was previously shown to be part of a gliosis-related tissue damage response in astrocytes (Zamanian et al., 2012). Moreover, we showed CXCL10 upregulation in both murine and human metastases-associated astrocytes *in vivo*. Notably, CXCL10 expression was evident in astrocytes that were physically in juxtaposition to brain-metastasizing melanoma cells and was already detectable in micrometastases, confirming our previous findings that neuroinflammation is an early event during the formation of brain metastases (Schwartz et al., 2016). CXCL10 was previously demon-

strated to be induced in human melanoma cells (Mauldin et al., 2015), and its levels were found to be elevated in the cerebrospinal fluid (CSF) of patients with melanoma brain metastases (Lok et al., 2014). However, the functional role of astrocyte-derived CXCL10 in facilitating brain metastasis was unresolved. We found that tumor cell-induced upregulation of CXCL10 in astrocytes resulted in the enhanced migration of melanoma cells toward astrocytes, which was attenuated when CXCL10 was inhibited. Silencing CXCL10 in melanoma cells also attenuated their migration. Previous studies implicated autocrine signaling by melanoma-derived CXCL10 in tumor progression and metastasis (Mauldin et al., 2015; Wightman et al., 2015). Thus, the migration of melanoma cells is mediated via both autocrine and paracrine signaling by activated astrocytes. Of note, while *in vivo* CXCL10 may be secreted by multiple cell types, including microglia, tumor cells, and astrocytes (Liu et al., 2011), in our *in vitro* experiments, astrocytes were the only source of CXCL10. Thus, our findings confirm the function of astrocyte-derived CXCL10 in the chemoattraction of melanoma cells.

To characterize melanoma brain tropism, we generated brain-tropic cells (sBT-RMS) from spontaneous brain metastases. When injected orthotopically, sBT-RMS cells were more aggressive in the formation of brain metastases compared to the parental melanoma cells, confirming their brain tropism *in vivo*.

Chemokine receptors were previously suggested to be upregulated in brain metastatic melanoma cells (Izraely et al., 2010). We show that CXCL10 neutralization attenuated the migration of brain-tropic melanoma cells (sBT-RMS) toward astrocytes, and that CXCR3, the receptor of CXCL10, is upregulated in sBT-RMS cells compared with the RMS parental cells. Moreover, sBT-RMS cells had an advantage in forming brain metastases while forming fewer lung metastases *in vivo*, indicating that CXCR3 expression endows melanoma cells with an advantage in forming brain metastases. We further show that abrogating the expression of CXCR3 by shRNA transduction or by nanoparticle-mediated siRNA delivery significantly inhibited melanoma cell migration toward astrocytes *in vitro*. Targeting the expression of CXCR3 profoundly inhibited infiltration into the brain parenchyma in a 3D *ex vivo* brain tissue model and the incidence of brain metastasis *in vivo*. Furthermore, CXCR3 overexpression facilitated the formation of metastases *in vivo*. These findings implicate a functional role for astrocyte-derived CXCL10 in facilitating melanoma brain metastasis.

### Figure 5. CXCR3 Is Functionally Important for the Formation of Melanoma Brain Metastases

- (A) Representative images of the organotypic co-culture tumor plug-brain slice interface, with SC-RMS and sh1-CXCR3 cells. Melanoma cells (mCherry, red), astrocytes (GFAP, green), and microglia (ILB4, magenta). Scale bars, 20  $\mu$ m.
- (B) Quantification of infiltrated SC-RMS or sh1-CXCR3 cells in (A);  $n = 12$  per group. Chi-square test; \* $p = 0.04$ .
- (C) Experimental design of intracardiac injections of CXCR3-KD and SC-RMS control cells.
- (D) Representative brain CT images (coronal) of mice injected with SC-RMS or CXCR3-KD cells. BV, blood vessel; Met, metastases. Scale bar, 5 mm. Additional CT images are shown in Figures S5D and S5E.
- (E) Representative images of brain macrometastases (midsagittal plane). Scale bar, 5 mm.
- (F) Staining of astrocytes (GFAP, digitally colored green) in brain sections of SC-RMS or sh1-CXCR3-injected mice (melanoma cells [mCherry, red]). Representative images of multiple fields analyzed from  $n = 3$  mice per group. Scale bars, 25  $\mu$ m.
- (G) Brain metastatic load analyzed by qPCR of mCherry. The cutoff for macrometastases was determined as  $2 \times SD \times 10^2$  and was combined with gross inspection findings (see Method Details). SC-RMS:  $n = 23$ , sh1-CXCR3:  $n = 22$ , sh2-CXCR3:  $n = 22$ , from  $n = 2$  independent biological repeats.
- (H) Brain metastasis incidence of mice analyzed in (G): percentages of micro- and macrometastases in each treatment group.
- (I) The CXCL10-CXCR3 axis in brain tropism: melanoma soluble factors induce CXCL10 secretion by astrocytes. CXCL10 signaling supports the brain invasion and colonization of CXCR3-expressing melanoma cells. This figure was designed using graphical elements from BioRender.

The migration of effector T cells into melanoma tumors was shown to depend on the presence of CXCL10-producing CD103<sup>+</sup> dendritic cells in a mouse model of melanoma and in human samples of metastatic melanoma (Spranger et al., 2017). However, while CXCL10 was previously implicated in the recruitment of effector T cells to the brain in inflammatory diseases (Ryu et al., 2015) and in primary CNS tumors (De Waele et al., 2017), its function in recruiting T cells to brain metastases is unknown. Our data indicate that T cells are mobilized by astrocyte-derived CXCL10, and staining *in vivo* confirmed that T cells were found in greater abundance in metastases-bearing brains in comparison to normal brains. While the CXCL10 pathway is not exclusively responsible for T cell recruitment, our data suggest that its physiological function in T cell recruitment is hijacked by melanoma cells to mediate their brain tropism.

The high density of CD3<sup>+</sup> or CD8<sup>+</sup> T cells was shown to be correlated with better overall survival in patients with brain metastases (Berghoff et al., 2013, 2015a). Moreover, CXCR3 expression on cytotoxic T lymphocyte (CTLs) was shown to enhance the therapeutic response to anti-PD-1 treatment in a mouse model of melanoma (Chheda et al., 2016). The expression of CXCR3 on NK cells was also shown to be important for CXCL10-induced chemoattraction in the anti-tumor response against solid melanoma tumors (Kim et al., 2018; Wennerberg et al., 2015). Therefore, future therapeutic targeting of CXCR3 aiming to interfere with astrocyte-melanoma cell crosstalk will need to be carefully designed to be tumor cell specific to avoid the abrogation of effector T cell recruitment to the brain.

In summary, we found that neuroinflammation, physiologically instigated as a protective response of astrocytes to overcome brain tissue damage, is hijacked by brain-metastasizing tumor cells to promote their metastatic capacity. CXCL10, which physiologically promotes immunity by recruiting effector T cells, supports the brain tropism of CXCR3-expressing melanoma cells and attracts melanoma cells to the metastatic site. Thus, reciprocal interactions between metastasizing melanoma cells and astrocytes are an important determinant in brain metastases. These findings suggest that the CXCL10-CXCR3 axis is a potential target for disrupting the formation of a pro-metastatic neuro-inflammatory brain niche and for preventing melanoma brain metastatic relapse.

## STAR★METHODS

Detailed methods are provided in the online version of this paper and include the following:

- **KEY RESOURCES TABLE**
- **LEAD CONTACT AND MATERIALS AVAILABILITY**
- **EXPERIMENTAL MODEL AND SUBJECT DETAILS**
  - Melanoma cell culture
  - Ethical statement for use of animals
  - Isolation of adult mouse primary astrocytes
  - Spontaneous melanoma brain metastasis model
  - Spontaneous brain-tropic and lung-tropic RMS cell lines
  - Intracranial injections
  - Experimental metastases by intracardiac injections

- Brain organotypic co-cultures
- Human subjects

- **METHOD DETAILS**

- Astrocyte purity analysis by immunocytochemistry (ICC)
- Astrocyte purity analysis by FACS
- Astrocyte purity analysis by qRT-PCR
- *In vitro* astrocyte activation by melanoma-CM
- Cytokine array
- ELISA assay
- Sorting metastases-associated astrocytes (MAA)
- Brain tissue preparation for histology
- Immunofluorescent tissue staining
- RNA extraction
- Quantitative real-time PCR (qRT-PCR)
- Melanoma migration assay
- T cell isolation and migration assay
- RMS CXCR3 transduction
- CXCR3 analysis by FACS
- Polyplex formation and electrophoretic mobility shift assay (EMSA)
- Dynamic light scattering (DLS) and zeta potential determination
- Plasma stability assay
- Cell viability assay
- APA: CXCR3 siRNA silencing
- siRNA migration assays
- Computed tomography (CT)

- **QUANTIFICATION AND STATISTICAL ANALYSIS**

## SUPPLEMENTAL INFORMATION

Supplemental Information can be found online at <https://doi.org/10.1016/j.celrep.2019.07.033>.

## ACKNOWLEDGMENTS

This work was supported by a grant from the Melanoma Research Alliance (MRA) to N. Erez, R.S.-F., and R.G. (the MRA-Saban Family Team Award) and by a grant from the German Research Foundation (DFG PU 355/4-1) to N. Erez and T.P. N. Erez and R.S.-F. thank the Gail White and Ann and William Cohen Multidisciplinary Brain Cancer Research Program. N. Erez is supported by funding from the European Research Council (ERC) under the European Union's Horizon 2020 research and innovation programme (starter grant agreement no. 637069 MetCAF). T.P. is supported by the German Research Foundation (DFG FOR2127 PU 355/5-1). R.S.-F. is also supported by the ERC under the European Union's Seventh Framework Programme/ERC Consolidator grant agreement no. [617445]-PolyDorm. The authors would like to thank the Sackler Interdepartmental Core Facility (SICF) for help with imaging, FACS, and qPCR analyses. H.D. acknowledges the Foulkes Foundation MD/PhD fellowship.

## AUTHOR CONTRIBUTIONS

Conceptualization, H.D., M.A. and N. Erez; Methodology, H.D., M.A. and N. Erez; Investigation, H.D., M.A., N. Ershaid, M.Y., R.B., T.G.L., Z.H., S.P., A.S., and J.C.; Formal Analysis, O.S., L.M., N.C., and G.T.; Resources, M.Y., O.A., R.G., and R.S.-F.; Visualization, H.D., M.A., and N. Erez; Writing – Original Draft, H.D., M.A., and N. Erez; Writing – Review & Editing, H.D., M.A., and N. Erez; Project Administration, T.P., C.L., R.S.-F., and N. Erez; Supervision, N. Erez. All of the authors discussed the results and provided feedback on the manuscript.

## DECLARATION OF INTERESTS

The authors declare no competing interests.

Received: January 7, 2019

Revised: June 20, 2019

Accepted: July 11, 2019

Published: August 13, 2019

## REFERENCES

- Amit, M., Laider-Trejo, L., Shalom, V., Shabtay-Orbach, A., Krelin, Y., and Gil, Z. (2013). Characterization of the melanoma brain metastatic niche in mice and humans. *Cancer Med.* 2, 155–163.
- Ankeny, J.S., Labadie, B., Luke, J., Hsueh, E., Messina, J., and Zager, J.S. (2018). Review of diagnostic, prognostic, and predictive biomarkers in melanoma. *Clin. Exp. Metastasis* 35, 487–493.
- Arnold, M., Holterhues, C., Hollestein, L.M., Coebergh, J.W., Nijsten, T., Pukkala, E., Holleczeck, B., Tryggvadóttir, L., Comber, H., Bento, M.J., et al. (2014). Trends in incidence and predictions of cutaneous melanoma across Europe up to 2015. *J. Eur. Acad. Dermatol. Venereol.* 28, 1170–1178.
- Baron, J.L., Madri, J.A., Ruddle, N.H., Hashim, G., and Janeway, C.A., Jr. (1993). Surface expression of alpha 4 integrin by CD4 T cells is required for their entry into brain parenchyma. *J. Exp. Med.* 177, 57–68.
- Berghoff, A.S., Lassmann, H., Preusser, M., and Höftberger, R. (2013). Characterization of the inflammatory response to solid cancer metastases in the human brain. *Clin. Exp. Metastasis* 30, 69–81.
- Berghoff, A.S., Fuchs, E., Ricken, G., Mlecnik, B., Bindea, G., Spanberger, T., Hackl, M., Widhalm, G., Dieckmann, K., Prayer, D., et al. (2015a). Density of tumor-infiltrating lymphocytes correlates with extent of brain edema and overall survival time in patients with brain metastases. *Oncolimmunology* 5, e1057388.
- Berghoff, A.S., Ricken, G., Widhalm, G., Rajky, O., Dieckmann, K., Birner, P., Bartsch, R., Höller, C., and Preusser, M. (2015b). Tumour-infiltrating lymphocytes and expression of programmed death ligand 1 (PD-L1) in melanoma brain metastases. *Histopathology* 66, 289–299.
- Blazquez, R., and Pukrop, T. (2017). 3D Coculture Model of the Brain Parenchyma-Metastasis Interface of Brain Metastasis. *Methods Mol. Biol.* 1612, 213–222.
- Burda, J.E., and Sofroniew, M.V. (2014). Reactive gliosis and the multicellular response to CNS damage and disease. *Neuron* 81, 229–248.
- Cheng, W., and Chen, G. (2014). Chemokines and chemokine receptors in multiple sclerosis. *Mediators Inflamm.* 2014, 659206.
- Chheda, Z.S., Sharma, R.K., Jala, V.R., Luster, A.D., and Haribabu, B. (2016). Chemoattractant Receptors BLT1 and CXCR3 Regulate Antitumor Immunity by Facilitating CD8+ T Cell Migration into Tumors. *J. Immunol.* 197, 2016–2026.
- Chuang, H.N., Lohaus, R., Hanisch, U.K., Binder, C., Dehghani, F., and Pukrop, T. (2013a). Coculture system with an organotypic brain slice and 3D spheroid of carcinoma cells. *J. Vis. Exp.* (80) <https://doi.org/10.3791/50881>.
- Chuang, H.N., van Rossum, D., Sieger, D., Siam, L., Klemm, F., Bleckmann, A., Bayerlová, M., Farhat, K., Scheffel, J., Schulz, M., et al. (2013b). Carcinoma cells misuse the host tissue damage response to invade the brain. *Glia* 67, 1331–1346.
- De Waele, J., Marcq, E., Van Audenaerde, J.R., Van Loenhout, J., Deben, C., Zwaenepoel, K., Van de Kelft, E., Van der Planken, D., Menovsky, T., Van den Bergh, J.M., et al. (2017). Poly(I:C) primes primary human glioblastoma cells for an immune response invigorated by PD-L1 blockade. *Oncolimmunology* 7, e1407899.
- Denucci, C.C., Mitchell, J.S., and Shimizu, Y. (2009). Integrin function in T-cell homing to lymphoid and nonlymphoid sites: getting there and staying there. *Crit. Rev. Immunol.* 29, 87–109.
- Doron, H., Pukrop, T., and Erez, N. (2019). A Blazing Landscape: Neuroinflammation Shapes Brain Metastasis. *Cancer Res.* 79, 423–436.
- Engelhardt, B., and Ransohoff, R.M. (2005). The ins and outs of T-lymphocyte trafficking to the CNS: anatomical sites and molecular mechanisms. *Trends Immunol.* 26, 485–495.
- Erez, N., and Coussens, L.M. (2011). Leukocytes as paracrine regulators of metastasis and determinants of organ-specific colonization. *Int. J. Cancer* 128, 2536–2544.
- Gibori, H., Elyahu, S., Krivitsky, A., Ben-Shushan, D., Epshtein, Y., Tiram, G., Blau, R., Ofek, P., Lee, J.S., Ruppin, E., et al. (2018). Amphiphilic nanocarrier-induced modulation of PLK1 and miR-34a leads to improved therapeutic response in pancreatic cancer. *Nat. Commun.* 9, 16.
- Harlin, H., Meng, Y., Peterson, A.C., Zha, Y., Tretiakova, M., Slingluff, C., McKee, M., and Gajewski, T.F. (2009). Chemokine expression in melanoma metastases associated with CD8+ T-cell recruitment. *Cancer Res.* 69, 3077–3085.
- Hoshino, A., Costa-Silva, B., Shen, T.L., Rodrigues, G., Hashimoto, A., Tesic Mark, M., Molina, H., Kohsaka, S., Di Giannatale, A., Ceder, S., et al. (2015). Tumour exosome integrins determine organotropic metastasis. *Nature* 527, 329–335.
- Izraely, S., Klein, A., Sagi-Assif, O., Meshel, T., Tsarfaty, G., Hoon, D.S., and Witz, I.P. (2010). Chemokine-chemokine receptor axes in melanoma brain metastasis. *Immunol. Lett.* 130, 107–114.
- Jiang, H., Gebhardt, C., Umansky, L., Beckhove, P., Schulze, T.J., Utikal, J., and Umansky, V. (2015). Elevated chronic inflammatory factors and myeloid-derived suppressor cells indicate poor prognosis in advanced melanoma patients. *Int. J. Cancer* 136, 2352–2360.
- Joyce, J.A., and Pollard, J.W. (2009). Microenvironmental regulation of metastasis. *Nat. Rev. Cancer* 9, 239–252.
- Kim, S.J., Kim, J.S., Park, E.S., Lee, J.S., Lin, Q., Langley, R.R., Maya, M., He, J., Kim, S.W., Weihua, Z., et al. (2011). Astrocytes upregulate survival genes in tumor cells and induce protection from chemotherapy. *Neoplasia* 13, 286–298.
- Kim, J., Kim, J.S., Lee, H.K., Kim, H.S., Park, E.J., Choi, J.E., Choi, Y.J., Shin, B.R., Kim, E.Y., Hong, J.T., et al. (2018). CXCR3-deficient natural killer cells fail to migrate to B16F10 melanoma cells. *Int. Immunopharmacol.* 63, 66–73.
- Klein, A., Schwartz, H., Sagi-Assif, O., Meshel, T., Izraely, S., Ben Menachem, S., Bengaiev, R., Ben-Shmuel, A., Nahmias, C., Couraud, P.O., et al. (2015). Astrocytes facilitate melanoma brain metastasis via secretion of IL-23. *J. Pathol.* 236, 116–127.
- Krivitsky, A., Polyak, D., Scomparin, A., Elyahu, S., Ofek, P., Tiram, G., Kalinski, H., Avkin-Nachum, S., Feiner Gracia, N., Albertazzi, L., and Satchi-Fainaro, R. (2018). Amphiphilic poly( $\alpha$ )glutamate polymeric micelles for systemic administration of siRNA to tumors. *Nanomedicine (Lond.)* 14, 303–315.
- Levy, A., Blacher, E., Vaknine, H., Lund, F.E., Stein, R., and Mayo, L. (2012). CD38 deficiency in the tumor microenvironment attenuates glioma progression and modulates features of tumor-associated microglia/macrophages. *Neuro Oncol.* 14, 1037–1049.
- Liddel, S.A., and Barres, B.A. (2017). Reactive Astrocytes: Production, Function, and Therapeutic Potential. *Immunity* 46, 957–967.
- Liddel, S.A., Guttenplan, K.A., Clarke, L.E., Bennett, F.C., Bohlen, C.J., Schirmer, L., Bennett, M.L., Münch, A.E., Chung, W.S., Peterson, T.C., et al. (2017). Neurotoxic reactive astrocytes are induced by activated microglia. *Nature* 541, 481–487.
- Lifshitz, V., Benromano, T., Weiss, R., Bonga-Kanfi, S., and Frenkel, D. (2013). Insulin-degrading enzyme deficiency accelerates cerebrovascular amyloidosis in an animal model. *Brain Behav. Immun.* 30, 143–149.
- Lin, Q., Balasubramanian, K., Fan, D., Kim, S.J., Guo, L., Wang, H., Bar-Eli, M., Aldape, K.D., and Fidler, I.J. (2010). Reactive astrocytes protect melanoma cells from chemotherapy by sequestering intracellular calcium through gap junction communication channels. *Neoplasia* 12, 748–754.
- Liu, M., Guo, S., and Stiles, J.K. (2011). The emerging role of CXCL10 in cancer (Review). *Oncol. Lett.* 2, 583–589.
- Lok, E., Chung, A.S., Swanson, K.D., and Wong, E.T. (2014). Melanoma brain metastasis globally reconfigures chemokine and cytokine profiles in patient cerebrospinal fluid. *Melanoma Res.* 24, 120–130.

- Mauldin, I.S., Wang, E., Deacon, D.H., Olson, W.C., Bao, Y., and Slingluff, C.L., Jr. (2015). TLR2/6 agonists and interferon-gamma induce human melanoma cells to produce CXCL10. *Int. J. Cancer* *137*, 1386–1396.
- Metzemaekers, M., Vanheule, V., Janssens, R., Struyf, S., and Proost, P. (2018). Overview of the Mechanisms that May Contribute to the Non-Redundant Activities of Interferon-Inducible CXC Chemokine Receptor 3 Ligands. *Front. Immunol.* *8*, 1970.
- Nayak, L., Lee, E.Q., and Wen, P.Y. (2012). Epidemiology of brain metastases. *Curr. Oncol. Rep.* *14*, 48–54.
- Peinado, H., Lavotshkin, S., and Lyden, D. (2011). The secreted factors responsible for pre-metastatic niche formation: old sayings and new thoughts. *Semin. Cancer Biol.* *21*, 139–146.
- Peinado, H., Zhang, H., Matei, I.R., Costa-Silva, B., Hoshino, A., Rodrigues, G., Psaila, B., Kaplan, R.N., Bromberg, J.F., Kang, Y., et al. (2017). Pre-metastatic niches: organ-specific homes for metastases. *Nat. Rev. Cancer* *17*, 302–317.
- Pekny, M., Wilhelmsson, U., and Pekna, M. (2014). The dual role of astrocyte activation and reactive gliosis. *Neurosci. Lett.* *565*, 30–38.
- Phares, T.W., Stohlman, S.A., Hinton, D.R., and Bergmann, C.C. (2013). Astrocyte-derived CXCL10 drives accumulation of antibody-secreting cells in the central nervous system during viral encephalomyelitis. *J. Virol.* *87*, 3382–3392.
- Placone, A.L., Quiñones-Hinojosa, A., and Searson, P.C. (2016). The role of astrocytes in the progression of brain cancer: complicating the picture of the tumor microenvironment. *Tumour Biol.* *37*, 61–69.
- Polyak, D., Krivitsky, A., Scomparin, A., Eliyahu, S., Kalinski, H., Avkin-Nachum, S., and Satchi-Fainaro, R. (2017). Systemic delivery of siRNA by aminated poly( $\alpha$ )glutamate for the treatment of solid tumors. *J. Control. Release* *257*, 132–143.
- Priego, N., Zhu, L., Monteiro, C., Mulders, M., Wasilewski, D., Bindeman, W., Doglio, L., Martínez, L., Martínez-Saez, E., Ramón Y Cajal, S., et al. (2018). STAT3 labels a subpopulation of reactive astrocytes required for brain metastasis. *Nat. Med.* *24*, 1024–1035.
- Ryu, J.K., Petersen, M.A., Murray, S.G., Baeten, K.M., Meyer-Franke, A., Chan, J.P., Vagena, E., Bedard, C., Machado, M.R., Rios Coronado, P.E., et al. (2015). Blood coagulation protein fibrinogen promotes autoimmunity and demyelination via chemokine release and antigen presentation. *Nat. Commun.* *6*, 8164.
- Schwartz, H., Blacher, E., Amer, M., Livneh, N., Abramovitz, L., Klein, A., Ben-Shushan, D., Soffer, S., Blazquez, R., Barrantes-Freer, A., et al. (2016). Incipient Melanoma Brain Metastases Instigate Astrogliosis and Neuroinflammation. *Cancer Res.* *76*, 4359–4371.
- Skaper, S.D., Facci, L., Zusso, M., and Giusti, P. (2018). An Inflammation-Centric View of Neurological Disease: Beyond the Neuron. *Front. Cell. Neurosci.* *12*, 72.
- Sørensen, T.L., Trebst, C., Kivisäkk, P., Klaege, K.L., Majmudar, A., Ravid, R., Lassmann, H., Olsen, D.B., Strieter, R.M., Ransohoff, R.M., and Sellebjerg, F. (2002). Multiple sclerosis: a study of CXCL10 and CXCR3 co-localization in the inflamed central nervous system. *J. Neuroimmunol.* *127*, 59–68.
- Spranger, S., Dai, D., Horton, B., and Gajewski, T.F. (2017). Tumor-Residing Batf3 Dendritic Cells Are Required for Effector T Cell Trafficking and Adoptive T Cell Therapy. *Cancer Cell* *31*, 711–723.e4.
- Valiente, M., Ahluwalia, M.S., Boire, A., Brastianos, P.K., Goldberg, S.B., Lee, E.Q., Le Rhun, E., Preusser, M., Winkler, F., and Soffiatti, R. (2018). The Evolving Landscape of Brain Metastasis. *Trends Cancer* *4*, 176–196.
- Wang, L., Cao, L., Wang, H., Liu, B., Zhang, Q., Meng, Z., Wu, X., Zhou, Q., and Xu, K. (2017). Cancer-associated fibroblasts enhance metastatic potential of lung cancer cells through IL-6/STAT3 signaling pathway. *Oncotarget* *8*, 76116–76128.
- Wennerberg, E., Kremer, V., Childs, R., and Lundqvist, A. (2015). CXCL10-induced migration of adoptively transferred human natural killer cells toward solid tumors causes regression of tumor growth in vivo. *Cancer Immunol. Immunother.* *64*, 225–235.
- Wightman, S.C., Uppal, A., Pitroda, S.P., Ganai, S., Burnette, B., Stack, M., Oshima, G., Khan, S., Huang, X., Posner, M.C., et al. (2015). Oncogenic CXCL10 signalling drives metastasis development and poor clinical outcome. *Br. J. Cancer* *113*, 327–335.
- Zamanian, J.L., Xu, L., Foo, L.C., Nouri, N., Zhou, L., Giffard, R.G., and Barres, B.A. (2012). Genomic analysis of reactive astrogliosis. *J. Neurosci.* *32*, 6391–6410.

## STAR★METHODS

### KEY RESOURCES TABLE

REAGENT or RESOURCE	SOURCE	IDENTIFIER
<b>Antibodies</b>		
Rabbit anti-Glial Fibrillary Acidic Protein (Multipurpose) antibody	Agilent	Cat# Z0334; RRID: AB_10013382
Goat anti-Mouse Cxcl10 / ip-10 / crg-2 Polyclonal antibody, Unconjugated	R&D Systems	Cat# AF-466-NA; RRID: AB_2292487
Rat anti-Mouse CD3 Monoclonal antibody, Unconjugated, Clone KT3	Bio-Rad	Bio-Rad Cat# MCA500GA; RRID: AB_323775
Rat anti-CD104 Monoclonal Antibody, Unconjugated, Clone 346-11A	BD Biosciences	Cat# 553745; RRID: AB_395027
Rat anti-mouse Nidogen (ELM1) antibody	Santa Cruz Biotechnology	Cat# sc-33706; RRID: AB_627519
Rabbit anti-mCherry antibody	Abcam	Cat# ab167453; RRID: AB_2571870
Mouse anti-human IP10 antibody [6D4]	Abcam	Cat# ab8098; RRID: AB_306267
Mouse anti-human CXCR3 antibody [2Ar1]	Abcam	Cat# ab64714, RRID: AB_1141480
Alexa Fluor 647-AffiniPure Donkey Anti-Rabbit IgG (H+L) (min X Bov,Ck,Gt,GP,Sy Hms,Hrs,Hu,Ms, Rat,Shp Sr Prot) antibody	Jackson ImmunoResearch Labs	Cat# 711-605-152; RRID: AB_2492288
Donkey anti-goat Dylight 488 antibody	Jackson ImmunoResearch Labs	Cat# 705-486-147; RRID: AB_2616594
Alexa Fluor® 488-AffiniPure Donkey Anti-Rabbit IgG (H+L) antibody	Jackson ImmunoResearch Labs	Cat# 711-545-152; RRID: AB_2313584
Alexa Fluor 647-AffiniPure Donkey Anti-Rat IgG (H+L) (min X Bov,Ck,Gt,GP,Sy Hms,Hrs,Hu,Ms,Rb,Shp Sr Prot) antibody	Jackson ImmunoResearch Labs	Cat# 712-605-153; RRID: AB_2340694
Donkey anti-Rat IgG (H&L) - Affinity Pure, DyLight®488 Conjugate antibody	Jackson ImmunoResearch Labs	Cat# DkxRt-003-D488NHSX; RRID: AB_2749829
Rhodamine Red-X-AffiniPure Donkey Anti-Rabbit IgG (H+L) (min X Bov,Ck,Gt,GP,Sy Hms,Hrs,Hu,Ms,Rat, Shp Sr Prot) antibody	Jackson ImmunoResearch Labs	Cat# 711-295-152; RRID: AB_2340613
Goat Anti-Rabbit IgG H&L (Alexa Fluor® 488) antibody	Abcam	Cat# ab150077; RRID: AB_2630356
Goat Anti-Mouse IgG H&L (Alexa Fluor 647) Antibody	Abcam	Cat# ab150115; RRID: AB_2687948
Rat Anti-Mouse Cxcr3 Monoclonal antibody, Allophycocyanin Conjugated, Clone 220803	R&D Systems	Cat# FAB1685A; RRID: AB_357071
Rat IgG2A Allophycocyanin Isotype Control (Clone 54447) antibody	R&D Systems	Cat# IC006A; RRID: AB_357254
Anti-ACSA-2-APC, mouse antibody	Miltenyi Biotec	Cat# 130-102-315; RRID: AB_2651190
Anti-Mouse CD45 FITC	Thermo Fisher Scientific	Cat# 11-0451-81; RRID: AB_465049
CD45 Monoclonal Antibody (30-F11), PE-Cyanine7, eBioscience	Thermo Fisher Scientific	Cat# 25-0451; RRID:AB_469625
CD11b Monoclonal Antibody (M1/70), PerCP-Cyanine5.5, eBioscience	Thermo Fisher Scientific	Cat# 45-0112-82; RRID: AB_953560
CD16/CD32 Monoclonal Antibody (93), eBioscience	Thermo Fisher Scientific	Cat# 14-0161-86; RRID:AB_467135
<b>Biological Samples</b>		
Patient-derived melanoma brain metastases tissues	Tel Aviv Sourasky Medical Center, institutional review board 0735-12-TLV	N/A
<b>Critical Commercial Assays</b>		
Mouse Cytokine Array Panel	R&D Systems	Cat# ARY006
Mouse CXCL10/IP-10 Quantikine ELISA kit	R&D Systems	Cat# MCX10
Fixation/Permeabilization Solution Kit	BD Biosciences	Cat# 554714

(Continued on next page)

<b>Continued</b>		
REAGENT or RESOURCE	SOURCE	IDENTIFIER
Experimental Models: Cell Lines		
Ret-melanoma sorted (RMS) cells	<a href="#">Schwartz et al., 2016</a>	N/A
Spontaneous brain-tropic RMS (sBT-RMS) cells	This paper	N/A
Spontaneous lung-tropic RMS (sLT-RMS) cells	This paper	N/A
Brain-tropic RMS (BT-RMS) cells	<a href="#">Schwartz et al., 2016</a>	N/A
Experimental Models: Organisms/Strains		
5-8-week-old male C57BL/6RCC mice	Envigo, Israel	N/A
Oligonucleotides		
See <a href="#">Table S1</a> . List of qRT-PCR primers	Hylabs	N/A
Scramble control shRNA sequence GCTTCGCG CCGTAGTCTTA	GeneCopoeia	N/A
sh1-CXCR3 shRNA sequence GGTTAGTGAACG TCAAGTGCT	GeneCopoeia	N/A
sh2-CXCR3 shRNA sequence TCAGCCTGAACT TTGACAGAA	GeneCopoeia	N/A
sh1-CXCL10 shRNA sequence TAGATTCCGGA TTCAGACATC	<a href="#">Wightman et al., 2015</a>	N/A
sh2-CXCL10 shRNA sequence TTGATGGTCTT AGATTCCGGA	<a href="#">Wightman et al., 2015</a>	N/A
Cxcr3-siRNA 13.1: CUAGAAACCUCACUUAAA CUUUCAA	Integrated DNA Technologies	N/A
Cxcr3-siRNA 13.3: CGUUUUCGAGCUAUGAGG CUAGUGG	Integrated DNA Technologies	N/A
Software and Algorithms		
ImageJ	NIH and LOCI, University of Wisconsin	<a href="https://imagej.nih.gov/ij/">https://imagej.nih.gov/ij/</a>
GraphPad Prism version 7.00 for Windows	GraphPad Software, La Jolla California USA	<a href="https://www.graphpad.com">https://www.graphpad.com</a>
BioRender	Information Technology Company, Toronto, Ontario	<a href="https://biorender.com/">https://biorender.com/</a>

## LEAD CONTACT AND MATERIALS AVAILABILITY

Further information and requests for resources and reagents should be directed to and will be fulfilled by the Lead Contact, Neta Erez ([netaerez@tauex.tau.ac.il](mailto:netaerez@tauex.tau.ac.il)).

## EXPERIMENTAL MODEL AND SUBJECT DETAILS

### Melanoma cell culture

RMS (Ret-melanoma sorted) cells ([Schwartz et al., 2016](#)), their derivative organ-tropic and transduced cell lines were grown in RPMI media (01-100-1A, BI) supplemented with 10% FCS, 1% Sodium Pyruvate (03-042-1B, BI) and 1% Penicillin-Streptomycin (03-031-1B, BI), at 37°C and 5% CO<sub>2</sub>. Melanoma cell lines were routinely tested for mycoplasma using the EZ-PCR Mycoplasma test kit (20-700-20, BI).

### Ethical statement for use of animals

All experiments involving animals were approved by the Tel Aviv University Institutional Animal Care and Use Committee (IACUC approval # 01-16-106). 5-8-week-old male C57BL/6RCC (Envigo, Israel) mice were maintained at the SPF facility of the Tel Aviv University or in the conventional animal facilities of the University of Regensburg (Germany).

### Isolation of adult mouse primary astrocytes

Isolation of mouse primary astrocytes was performed as previously described ([Lifshitz et al., 2013](#); [Schwartz et al., 2016](#)). 5-6-week-old C57/BL6 male mice were euthanized and their brains were harvested, minced and dissociated to single cell suspensions in collagenase type-III (LS004182, Worthington Biochemical Corporation) and dispase (04942078001, ROCHE). Demyelination was

achieved using percoll (P4937-500ML, Sigma-Aldrich). Isolated cells were seeded in 24 well plates pre-coated with poly-D-lysine (P7405, Sigma), and cultured in RPMI media supplemented with 10% FCS, 1% Sodium Pyruvate and 1% Penicillin-Streptomycin, at 37°C and 5% CO<sub>2</sub>. All experiments were performed on low passage (p2-5) cells.

### Spontaneous melanoma brain metastasis model

We utilized our previously established spontaneous model of melanoma brain metastasis (Schwartz et al., 2016). A total of  $5 \times 10^5$  RMS or sBT-RMS cells were re-suspended in PBS and mixed 1:1 with growth factor-reduced Matrigel (356231, BD Biosciences) to a final volume of 50 $\mu$ L. Mice were anesthetized by isoflurane, and a 29G insulin syringe (BD Biosciences) was used to perform subdermal injections at the right flank. Tumors were measured every other day using calipers, and tumor volumes were calculated using the formula  $X^2 \times Y \times 0.5$  (X-smaller diameter, Y-larger diameter). Tumors were excised 2 weeks later, following anesthesia with ketamine (100 mg/kg) xylazine (10 mg/kg). An incision was made in the skin adjacent to the tumor and it was dissected with clean margins. Tumor-associated connective tissue and blood vessels were also detached to prevent recurrence, and the incision was sutured using vicryl threads (J304H, ETHICON). Mice were weighed twice weekly and monitored until relapse or euthanasia.

### Spontaneous brain-tropic and lung-tropic RMS cell lines

Following subdermal injection of RMS cells, and primary tumor excision, mice were monitored for spontaneous lung or brain macrometastases. Overt macrometastases from lungs and brains (~6 months after primary tumor removal) were dissected, cut into small pieces, cultured for a week, and treated with 2 $\mu$ g/ml Puromycin (MegaPharm, P-1033-SOL), to select for mCherry-expressing melanoma cells. The cells isolated from brain and lungs were designated sBT-RMS (spontaneous brain-tropic RMS) and sLT-RMS (spontaneous lung-tropic RMS), respectively. Cells were then injected subdermally and monitored closely following primary tumor excision, as described above. Mice were euthanized 1.5 months post tumor excision, and brains were harvested for RNA extraction and qPCR analysis of metastases, which validated the organ-specific metastatic capability of the established cell lines.

### Intracranial injections

8-week-old male C57BL/6 mice were anesthetized by isoflurane and placed in a Kopf Stereotaxic Alignment System. 500 RMS cells in 3 $\mu$ L RPMI were injected as previously described (Levy et al., 2012; Schwartz et al., 2016). RPMI SFM was injected as control. Macrometastases-bearing brains were harvested 5 days later and processed for histology or FACS analysis as described below.

### Experimental metastases by intracardiac injections

8-week-old male C57BL/6 mice were anesthetized with ketamine/xylazine. Mice were placed under a small animal ultrasound (Vevo 770 High-Resolution *In Vivo* Micro-Imaging System; VisualSonics Inc.).  $10^5$  RMS cells in 100 $\mu$ L PBS were inoculated into the left ventricle of the heart using a 29G needle. Mice were weighed every other day. Mice injected with RMS CXCR3-KD cells underwent CT imaging 9 days after injections and were euthanized on day 10. Brains were harvested and hemisected in the midsagittal plane for gross inspection of macrometastases. Brains were flash frozen for RNA extraction and qPCR analysis of metastases. Three representative hemispheres from each group were taken for histological analysis. Mice injected with RMS CXCR3 OE underwent CT imaging 14 days after injections and were euthanized on the same day. Total brain RNA was extracted, and brain metastatic load was assessed by qPCR of mCherry expression, as described below. Metastasis positivity threshold was set at  $2 \times$  SD above the mean expression in normal control brains. The threshold for macrometastases was set at  $2 \times$  SD  $\times 10^2$  above the mean expression in normal control brains. The final cutoff for macrometastases included the detection of macrometastases by gross inspection or by CT.

### Brain organotypic co-cultures

These experiments were performed with RMS, sBT-RMS, sLT-RMS, SC-RMS and CXCR3-KD cells, as previously described (Blazquez and Pukrop, 2017; Chuang et al., 2013a). Brains were sliced horizontally into 350  $\mu$ m sections using a vibratome. Organotypic brain slices were placed on a 0.4  $\mu$ m polycarbonate transwell membrane insert in a 6 well plate with 1ml cultivation medium in the lower well.  $10^5$  tumor cells were embedded in 20  $\mu$ L gel matrix of 30% RPMI medium and 70% ECM gel. RMS-gel matrix mix was placed into a sterile metallic spacer (3.8mm diameter) adjacent to the cortical region of the organotypic brain slice and incubated for 1h. The spacer was removed, and the 3D tumor spheroid was left to co-culture with the brain slice for 4 days. Immunofluorescent staining of astrocytes and microglia in the organotypic brain slice was performed. Tumor infiltration grade was determined using a scoring system: 0 = no infiltration; + < 1/3; ++ = 1/3 - 2/3; +++  $\geq$  2/3 of the contact area infiltrated by tumor cells.

### Human subjects

Patient-derived melanoma brain metastases tissues were collected after written informed consent was obtained from the research subjects (males, aged 58 and 62) by the Tel Aviv Sourasky Medical Center, under an approved institutional review board (IRB) (0735-12-TLV).

## METHOD DETAILS

### Astrocyte purity analysis by immunocytochemistry (ICC)

Primary astrocytes ( $5 \times 10^4$  per well) were seeded onto glass coverslips that were pre-coated with poly-D-lysine, in 24 well plates. Cells were fixed with 4% PFA for 20min on ice, permeabilized with 0.2% triton for 2min, thoroughly washed, incubated in 10% donkey serum for 30min, and stained with rabbit anti-GFAP (1:500, Z-0334, Agilent), for 1h at room temperature. Cells were then washed and incubated with Alexa Fluor 488-conjugated donkey anti-rabbit antibody (1:500, 711-545-152, Jackson) for 30min. For CD11b staining, Fc block (1:50, CD16/CD32 Monoclonal Antibody, 14-0161-86, eBioscience) was applied for 30min, followed by staining with CD11b-FITC (1:100, 11-01-02 eBioscience) for 1.5h. The coverslips were mounted with DAPI onto microscope slides. Astrocyte purity was confirmed, as all cells were stained positive for GFAP and negative to microglia marker CD11b.

### Astrocyte purity analysis by FACS

For intracellular GFAP staining of cultured primary astrocytes, cells were collected, suspended with Fc block (1:50, CD16/CD32 Monoclonal Antibody, 14-0161-86, eBioscience) in FACS buffer (1% FCS in PBS) and incubated for 40min. Cells were then fixed and permeabilized using the Fixation/Permeabilization Solution Kit (554714, BD Biosciences), according to the manufacturer's instructions. Following blocking with 2% donkey serum in FACS buffer, the cells were incubated with 50 $\mu$ L BD Perm/Wash buffer with the GFAP antibody (1:100, Z-0334, Agilent) for 30min at 4°C in the dark, with gentle mixing every 2-5min to prevent clumping and maximize staining efficacy. Cells were then washed and incubated with secondary antibody donkey anti-rabbit 647 (1:500, 711-605-152, Jackson) for 30min. For membranous CD45 and CD11b staining, cells were incubated with a mix of 1:50 Fc block, CD45-PE-Cy7 (1:200, 25-0451-82, eBioscience) and CD11b-PerCP-Cy5.5 (1:250, 45-0112-82, eBioscience) in FACS buffer for 30min. Prior to FACS analysis, cells were fixed with 4% PFA, washed and re-suspended in FACS buffer. All incubations took place at 4°C, in the dark, and suitable isotype controls were included for each sample. Flow cytometry was performed using CytoFLEX Platform and data were analyzed using Kaluza 1.2 and FlowJo®. Astrocyte purity was confirmed as 98.7% GFAP-positive, and 99.6% negative to immune cell and microglia markers.

### Astrocyte purity analysis by qRT-PCR

RNA was extracted from cultured astrocytes and analyzed for the expression of *Gfap* and *Cd11b*. Cultured splenocytes from dissociated spleens were used as control. Reverse transcription and qRT-PCR analysis were performed as described below. Astrocytes were shown to express *Gfap*, while microglia marker *Cd11b* expression was undetected.

### In vitro astrocyte activation by melanoma-CM

To prepare melanoma-conditioned media (CM),  $2 \times 10^5$  RMS or SBT-RMS cells were seeded in 10cm plates and incubated for 48h in serum-free media (SFM). Melanoma-CM was collected, filtered with 0.2  $\mu$ m filter (Millipore) and used fresh.  $3 \times 10^5$  astrocytes/well were seeded in 6 well plates for 24h. Astrocytes were then incubated with melanoma-CM or SFM control for 16h, then washed with PBS and incubated in fresh SFM for an additional 24h to produce activated astrocyte-CM or normal astrocyte-CM respectively.

### Cytokine array

Normal or RMS-activated astrocytes were prepared as above and lysed. 200  $\mu$ g from each sample was hybridized with the Mouse Cytokine Array Panel (ARY006, R&D). Results were quantified by the ImageJ software.

### ELISA assay

Normal or RMS-activated astrocytes were prepared as above. Media were concentrated using Amicon Ultra-15 Centrifugal Filter Units 3kDa (MMUFC900324, Millipore) and analyzed in duplicates. Mouse CXCL10/IP-10 Quantikine ELISA kit was used according to the manufacturer's instructions (MCX10, R&D). Results were normalized to cell numbers.

### Sorting metastases-associated astrocytes (MAA)

Normal and experimental macrometastases-bearing brains were digested with collagenase/dispase, demyelinated and stained with ACSA-2-APC (1:10, 130-102-315, Miltenyi Biotec) to collect astrocytes. Melanoma cells were excluded with mCherry, immune cells and microglia were excluded with CD45-FITC (1:200, 11-0451-81, eBioscience) and CD11b-PerCP-Cy5.5 (1:250, 45-0112-80, eBioscience). Sorting was performed with the BD-FACSAria-II. Astrocyte purity was validated by qPCR analysis of cell type-specific markers.

### Brain tissue preparation for histology

Mice were anesthetized with ketamine/xylazine, brains were harvested and washed in PBS, then cut in the midsagittal plane and examined by gross inspection for metastatic lesions. Brains were incubated for 5h in 4% PFA (Electron Microscopy Sciences) and transferred to 1% PFA overnight (O/N). Brains were incubated in 0.5M sucrose for 1h, then in 1M sucrose O/N. Brains were incubated in Optimal Cutting Temperature compound (OCT, Tissue-Tek) for 1h. All incubations were performed at 4°C. Brains were embedded in OCT on dry ice, then stored at  $-80^\circ\text{C}$ . 10  $\mu$ m serial sections were cut using a cryostat (CM1950, Leica), and slides were stored at  $-80^\circ\text{C}$ .

### Immunofluorescent tissue staining

Frozen brain tissue sections were incubated at 60°C for 20min, washed with PBS, then blocked with Protein block solution (X0909, DAKO) for 20min. Slides were incubated for 1.5h at RT with rabbit anti-mouse GFAP (Z-0334, Agilent), goat anti-mouse CXCL10 (AF-466-NA, R&D) or rat anti-mouse CD3 (MCA500GA, Bio-Rad), diluted 1:1000, 1:100, and 1:100, respectively. Fluorescently-conjugated secondary antibodies donkey anti-rabbit Alexa Fluor 647 (711-605-152, Jackson), donkey anti-goat Dylight-488 (705-486-147, Jackson), donkey anti-rat 647 (712-605-153, Jackson) diluted 1:1000 were applied for 30min at RT. Stained slides were mounted with DAPI Fluoromount-G (0100-20, Southern Biotech), left to dry O/N at RT and stored at 4°C. Images were acquired using the confocal Leica SP8 platform. For the ITGβ4 and nidogen stainings, rat anti-CD104 (553745, BD Biosciences), rabbit anti-mCherry antibody (b167453, Abcam) and rat anti-Nidogen (ELM1) antibody (sc-33706, Santa Cruz) were diluted 1:200, 1:500 and 1:2000 respectively, and fluorescently-conjugated donkey anti-rabbit rhodamine (711-295-152, Jackson) and donkey anti-rat DyLight-488 (DkxRt-003-D488NHSX, Jackson) diluted 1:1000 were applied for 30min at RT. Images were acquired using a Nikon C2+ laser-scanning confocal microscope with a 60 × /1.4 oil objective or a 20 × /0.75 air objective.

Human frozen OCT-embedded melanoma brain metastases tissues were cryosectioned into 5μm sections. Immunostaining was performed using the BOND RX automated immunohistochemistry (IHC) stainer (Leica Biosystems). Slides were incubated in 10% goat serum and 0.02% Tween-20 in PBS for 30min. Rabbit anti-GFAP (1:500, Z0334, Agilent), mouse anti-human CXCL10 (IP10) (1:25, ab8098, Abcam) or mouse anti-human CXCR3 (1:100, ab64714, Abcam) antibodies were applied for 1h. Secondary antibodies goat anti-rabbit Alexa 488 (1:300, b150077, Abcam), and goat anti-mouse Alexa-647 (1:300, ab150115, Abcam) were applied for 1h. Nuclei were counterstained with ProLong Gold antifade reagent with DAPI (Invitrogen). Images were captured using Evos FL Auto, Life Technologies microscope, at 40x magnification.

### RNA extraction

In all *in vivo* experiments, RNA was purified using EZ-RNA II kit (20-410-100, BI) according to the manufacturer's instructions. Total brains or lungs were homogenized in 1ml denaturation solution A in M tubes (130-096-335, Milteny Biotec) utilizing gentleMACS Dissociator (Milteny Biotec). For *in vitro* experiments, RNA was extracted using the PureLink RNA Mini Kit (12183018A, Invitrogen).

### Quantitative real-time PCR (qRT-PCR)

Reverse transcription was performed with qScript (95047-100, Quanta Biosciences) in all experiments. 10ng cDNA were used for *in vitro* experiments and 40ng were used for *in vivo* experiments. qRT-PCR analyses were conducted using PerfeCTa SYBR Green FastMix ROX (95073-012-4, Quanta Biosciences). Expression results were normalized to *Hprt* unless otherwise stated, and to the appropriate control group as indicated ( $RQ = 2^{-\Delta\Delta C_t}$ ).

See [Table S1](#). List of qRT-PCR primers.

### Melanoma migration assay

Melanoma cells were cultured in SFM for 48h prior to the experiment.  $1 \times 10^5$  astrocytes/well were seeded in 24 well plates and 24h later, incubated for 5h in SFM. 600μl SFM was added to the astrocytes (lower chamber) and 5μg/ml anti-CXCL10 (AF-466-NA, R&D) was added when indicated. 0.8μm pore transwell membrane inserts were placed in the astrocyte-containing wells and  $5 \times 10^4$  melanoma cells in 100μl SFM RPMI were seeded onto insert membranes (upper chamber). Experiments were run in duplicates. 48h later, transwell membranes were fixated with 4% PFA for 20min on ice, washed with PBS, and carefully cut out and mounted onto microscope slides with DAPI Fluoromount-G. Microscope pictures of membranes were taken, and migrated cells were analyzed with the ImageJ software.

### T cell isolation and migration assay

Spleens were harvested from 5-6-week-old C57/BL6 male mice, minced and dissociated. T cells were isolated using Magnisort Mouse T Cell Enrichment Kit (8804-6820-74).  $1 \times 10^6$  T cells in 100μl SFM RPMI were seeded onto 3μm pore size membranes of 24 well transwell inserts. The lower chamber contained SFM, normal astrocyte-CM, RMS-activated astrocyte-CM or sBT-RMS-activated astrocyte-CM (prepared as described above). Migration was assessed after 5h and experiments were run in duplicates. 5mM EDTA was added to all wells and media containing migrated cells was collected. Migrated cells were counted using a hemocytometer.

### RMS CXCR3 transduction

The expression of CXCR3 was knocked down in melanoma cells by lentiviral transduction of shRNA. LVRU6GH lentiviral plasmids containing shRNA for CXCR3 (sh1-CXCR3 GGTTAGTGAACGTCAAGTGCT and sh2-CXCR3 TCAGCCTGAACCTTTGACAGAA), or scrambled control (GCTTCGCGCCGTAGTCTTA) were purchased from GeneCopoeia. CXCL10 knockdown in melanoma cell lines was performed by cloning previously established (Wightman et al., 2015) shRNA sequences (sh1-CXCL10 TAGATTCCGGATT CAGACATC and sh2-CXCL10 TTGATGGTCTTAGATTCCGGA) into the LVRU6GH-backbone plasmid. Lentiviral transduction was performed as previously detailed (Schwartz et al., 2016). Overexpression of CXCR3 was achieved by lentiviral transduction of RMS cells with backbone plasmid, or with the CXCR3 ORF (Accession number GeneBank: NM\_009910, vector pEZLv152). Infected cells were selected with 2 μg/ml Puromycin and 100 μg/ml Hygromycin (H-270-5-1, ENCO). Validation of silencing was performed with qPCR prior to experiments.

### CXCR3 analysis by FACS

RMS, sBT-RMS or CXCR3-KD cells were incubated for 48h in SFM. Cells were collected following 5min incubation with PBS, centrifuged and counted.  $1 \times 10^6$  cells were resuspended in 100 $\mu$ l FACS buffer (0.5% FCS in PBS). Following blocking, mouse anti-CXCR3 APC antibody (1:10, FAB1685A, R&D) was added. Isotype controls (1:10, IC006A, R&D) and unstained controls were included for each sample. Dead cells were excluded either with DAPI (when cells were analyzed fresh) or Zombie viability dye (423113, BioLegend) when cells were analyzed following fixation with 4% PFA. Flow cytometry was performed using Gallios (Beckman Coulter, Brea, CA) and CytoFLEX Platform. Data were analyzed using Kaluza 1.2 and FlowJo®.

### Polyplex formation and electrophoretic mobility shift assay (EMSA)

Two sequences of siRNA against CXCR3 (Cxcr3-siRNA 13.1: CUAGAAACCUCACUUAACUUUCA or 13.3: CGUUUUCGAGCUAUGAGGCUAGUGG) designated siRNA-1 CXCR3 and siRNA-2 CXCR3, respectively, were purchased from IDT. Both siRNA sequences were complexed with amphiphilic poly( $\alpha$ )glutamate amine (APA) nanocarrier as previously described (Gibori et al., 2018), and designated APA:siRNA-1 CXCR3 and APA:siRNA-2 CXCR3 polyplexes. APA:siRNA targeting EGFP was used as negative control (NC). Evaluation of the optimal N/P ratio (amine groups of APA to phosphate groups of the siRNA) for complexation of APA with siRNA was performed. 50pmol of siRNA was mixed with increasing amounts of polymer and left to form complexes at room temperature for 30min. DNA loading buffer was added to the samples, which ran for 30min at 100V on a 2% agarose gel.

### Dynamic light scattering (DLS) and zeta potential determination

Samples were prepared at APA concentration of 0.1mg/ml in 15mM PBS, all measurements were performed at 25°C DLS and zeta potential measurements analysis was performed using Mobius (Wyatt Technology Corporation, Santa Barbara, CA, USA), equipped with a 532nm laser and a DLS Fluorescence Filter.

### Plasma stability assay

The stability of APA:Cxcr3-siRNA in plasma was evaluated by incubating the polyplexes in 50% mouse plasma for 0.5–24h and electrophoresis was performed as above. Naked siRNA at the same concentration was loaded as control.

### Cell viability assay

$1.5 \times 10^4$  RMS cells were seeded in 24 well plates. Cells were treated with APA:siRNA-1 CXCR3, APA:siRNA-2 CXCR3 or APA:NC-siRNA (N/P 2, 50nM) for 24h and counted.

### APA:CXCR3 siRNA silencing

The capability of APA:siRNA CXCR3 to inhibit *Cxcr3* at the mRNA level was assessed by treating melanoma cells with equivalent concentrations of 50nM siRNA in APA:siRNA CXCR3 nano-polyplex:  $2.5 \times 10^4$  RMS cells were seeded in 6 well plates and incubated for 24h with the polyplexes. RNA isolation and qPCR were performed as above.

### siRNA migration assays

Melanoma cells were incubated for 24h with the different polyplexes. Migration was analyzed after 24h by fixation and staining (Hema 3 Stain System; Fisher Diagnostics, USA). EVOS FL Auto microscope (Thermo Fisher scientific, USA) and ImageJ software were used for analysis.

### Computed tomography (CT)

Mice were anesthetized by an IP injection of ketamine (100 mg/kg) and xylazine (20 mg/kg), then received an IV injection of 200 $\mu$ L Omnipaque (iohexol 350mg/mL) to the tail vein. They were then placed in a TomoScape® Synergy micro-CT scanner at a resolution of 100 $\mu$ m, with the following parameters: 40kV X-ray voltage, scan time: 90 s; 3 gantry rotations, radiation dose: 322mGy/cm, each tube current: 1mAmp. After intracardiac inoculation, computed tomography brain images were acquired on day 9 for shCXCR3-injected mice, and day 14 for CXCR3 OE-injected mice. Identification of macrometastases was validated by multiple planar views of each suspected lesion and reviewed by a specialist radiologist.

## QUANTIFICATION AND STATISTICAL ANALYSIS

The statistical details of experiments, including statistical tests used, number of experiments and mice, can be found in the figure legends. Student's t test, One-way or Two-way ANOVA with Tukey's-post hoc test, or Chi-square were performed to analyze experiments, as appropriate, using GraphPad Prism version 7.00 for Windows. All analyses were two-tailed except for the ELISA result in Figure 1D and the qPCR in Figure 4F, which were one-tailed. Data were considered significant when *p*-value < 0.05.